Oblique basin inversion leads to fold localisation at bounding faults: Analogue modelling of the Achental structure, Northern Calcareous Alps, Austria

Willemijn S.M.T. van Kooten[1,2], Hugo Ortner[1], Ernst Willingshofer[3], Dimitrios Sokoutis[3,4], Alfred Gruber[5], Thomas Sausgruber[6]

[1]Institut für Geologie, Universität Innsbruck, Innsbruck, 6020, Austria
[2]Department of Management, Communication & IT, MCI Management Center Innsbruck, Innsbruck, 6020, Austria
[3]Department of Earth Sciences, Utrecht University, Utrecht, 3584 CB, Netherlands
[4]Department of Geosciences, University of Oslo, Oslo, Norway
[5]Geologische Bundesanstalt für Österreich (GBA), Wien, 1030, Austria
[6]die.wildbach, Wilhelm-Greil-Straße 9 6020 Innsbruck, Austria

Correspondence to: Willemijn S.M.T. van Kooten (willemijn.vankooten@mci.edu), ORCID: 0000-0002-9784-444X

Abstract

Within the Northern Calcareous Alps fold-and-thrust belt of the Eastern Alps, multiple deformation phases have contributed to the structural grain that localised deformation at later stages. In particular, Jurassic rifting and opening of the Alpine Tethys led to the formation of extensional basins at the northern margin of the Apulian plate. Subsequent Cretaceous shortening within the Northern Calcareous Alps produced the enigmatic Achental structure, which forms a sigmoidal transition zone between two E-W striking major synclines. One of the major complexities of the Achental structure is that all structural elements are oblique to the Cretaceous direction of shortening. It was therefore proposed to be a result of forced folding at the boundaries of the Achental basin. This study analyses the structural evolution of the Achental structure through integrating field observations with crustal-scale physical analogue models, to elucidate the influence of pre-existing crustal heterogeneities on oblique basin inversion and the prerequisites for the formation of a sigmoidal hanging wall that outlines former basin margins. From brittle-ductile models, we infer that shortening oblique to pre-existing extensional faults can lead to the localisation of thrust faults at the existing structure within a single deformation phase. Prerequisites are 1) a weak basal décollement that is offset by an existing normal fault, 2) the presence of topography in the hinterland, 3) a thin-skinned deformation style. Consequently, the Achental low-angle thrust and corresponding folds was able to localise exactly at the basin margin, with a vergence opposite to the Jurassic normal fault, creating the characteristic sigmoidal morphology during a single phase of NW-directed shortening.

1 Introduction

The deformational style and tectonic history of Earth's orogenic belts is strongly influenced by pre-existing structural elements. In particular, structures formed by shortening and inversion of pre-orogenic basins are often governed by the reactivation of former basin-bounding normal faults as summarised by Turner and Williams (2004) or Cooper and Warren (2020). Consequently, previous studies have focused on the mechanics of fault reactivation (e.g., Sibson 1995; Etheridge 1986; Tong and Yin 2011; Nielsen and Hansen 2000), or present regional case studies of basin inversion (e.g., Kley et al. 2005; Thorwart et al. 2021; Héja et al. 2022). Existing literature presenting analogue and numerical modelling of inversional settings is extensive and includes the re-activation of planar and listric extensional fault systems of various orientation as well as basin inversion orthogonal or oblique to the basin axes (e.g., Bonini 1998; Buiter and Pfiffner 2003; Amilibia et al. 2005; Buchanan and McClay 1992; Koopman et al. 1987; Konstantinovskaya et al. 2007; Sassi et al. 1993; Dubois et al. 2002; Zwaan et al. 2022; Brun and Nalpas 1996). In most models, newly formed reverse faults are synthetic to the pre-existing normal faults (see

40   also Bonini et al. 2012; their Figure 3), whereas the formation of thrust faults antithetic to the former basin-bounding faults is seldom described.

In this study, we use an example from the Northern Calcareous Alps (NCA) in Austria (Figure 1a), in which basin inversion during Alpine orogeny has created a low-angle thrust antithetic to a normal fault bounding a Jurassic extensional basin. In the hanging wall of this thrust, a fold train outlines the margins of this former basin, forming a characteristic sigmoidal shape that

45   has been the subject of geological investigations since the beginning of the 20th century (Ampferer 1902, 1941; Fuchs 1944; Nagel 1975; Nagel et al. 1976; Quenstedt 1933). We use the example of the Achental structure as a starting point for analogue modelling, to simulate the oblique inversion of a former extensional basin and the deformation of a brittle-ductile sedimentary succession at its margins. In particular, this study examines whether a sigmoidal hanging wall shape outlining former basin margins can be explained by a single phase of oblique shortening and if so what are the critical rheological and kinematic

50   parameters to obtain such structures. Our modelling results are then compared to the Achental structure, to better understand the formation of complex inversion structures in fold-and-thrust belts.

2 Geological setting

The Northern Calcareous Alps (NCA) of Austria (Figure 1a) have a polyphase tectonic and sedimentary history that started in the Permian. The following stages are distinguished:

55   1) Deposition on the south(east)ern passive margin of Pangaea bordering the Neotethys from the Permian to the end of the Triassic (e.g., Haas et al. 1995; Lein 1987; Schmid et al. 2004; Stampfli et al. 1998; Schmid et al. 2008). The major part of the Permian-Triassic is carbonate platforms.

    2) Early to Middle Jurassic rifting and subsequent opening of the Alpine Tethys that separated the Apulian/Adriatic microplate from the European continent (e.g., Faupl and Wagreich 1999; Schmid et al. 2004; Froitzheim and

60   Manatschal 1996). Rift-related subsidence caused the drowning of former Triassic carbonate platforms, rift-related faulting established the normal faults that were inverted during Cretaceous orogeny (Eberli et al. 1993; Ortner et al. 2008).

    3) Shortening related to Late Jurassic obduction of Neotethys oceanic crust onto the southeastern Apulian margin heralded inversion of this margin that culminated in Cretaceous orogeny (Schmid et al. 2004; Stüwe and Schuster

65   2010). During Cretaceous orogeny the NCA were a typical thin-skinned fold-and-thrust belt at the external margin of the Austroalpine orogenic wedge in lower plate position (Eisbacher and Brandner 1996; Ortner and Kilian 2022).

    4) During the Late Cretaceous this wedge was transported toward the northwestern passive margin of the Apulian plate. In the late Cretaceous, this margin became an active margin where the Alpine Tethys was subducted (Ortner and Sieberer 2022; Stüwe and Schuster 2010; Willingshofer et al. 1999).

70   5) Late Eocene closure of the Alpine Tethys caused collision between the lower, European and upper, Apulian plates and thus a second, Paleogene Alpine orogeny (Eisbacher and Brandner 1996; Schmid et al. 2004; Stüwe and Schuster 2010; Ortner 2003b). In the course of this process the Austroalpine units and the NCA fold-and-thrust belt were transported piggyback onto the European margin. Contrasting with Cretaceous orogeny, the Austroalpine wedge formed the upper plate during Paleogene orogeny.

75   The important stages in the frame of this study are Jurassic rifting that created basins, and Cretaceous and Paleogene shortening that led to basin inversion. Jurassic extensional basins formed along intersecting fault systems with N-S trending normal faults and E-W trending transform faults, as studied in the Eastern Alps of Switzerland (Eberli 1987, 1985; Weissert and Bernoulli 1985). Similar orientations of extensional normal faults have been found in the Western Alps (Lemoine et al. 1986). In the present-day Achensee region, Jurassic extension and the formation of an extensional basin is indicated by filled fissures that

80 occur in Oberrhätkalk (Gruber et al. 2022), strong lateral thickness variations of (Upper) Jurassic strata (Figure 1b) (Schütz 1979; Nagel et al. 1976) and characteristic breccias that are locally intercalated in basinal Jurassic sediments (Spieler and Brandner 1989; Channell et al. 1992; Channell et al. 1990; Brandner et al. 2011).

Cretaceous to Paleogene shortening within the NCA is characterized by two separate directions of transport. Whereas during Cretaceous orogeny the thrust sheets of the NCA were transported and stacked in WNW- to NW-direction (Eisbacher and

85 Brandner 1996), during Paleogene orogeny the NCA fold-and-thrust belt was transported in N- to NNE-direction (Schmid et al. 1996). The basement units of the Austroalpine wedge show a clear separation between the Cretaceous and Paleogene stages (Froitzheim et al. 1994), but synorogenic growth strata show continuous shortening within the NCA (Ortner 2001, 2003a; Ortner and Gaupp 2007; Ortner et al. 2016). The nappe structure of the NCA (Tollmann 1973; Hahn 1912, 1913b, 1913a; Ampferer and Hammer 1911; Ampferer 1912; Heißel 1958; Eisbacher and Brandner 1996; Tollmann 1970, 1976) has recently

90 been revised (Ortner 2016; Ortner and Kilian 2022). Consequently, the former Inntal and Lechtal thrust sheets have been combined in the Karwendel thrust sheet (Figure 1a), which overthrusts the Tannheim thrust sheet (combined from the Allgäu thrust sheet, Puitentalzone and Karwendelschuppenzone) to the north (Ortner 2016; Ortner and Kilian 2022; Kilian and Ortner 2019).
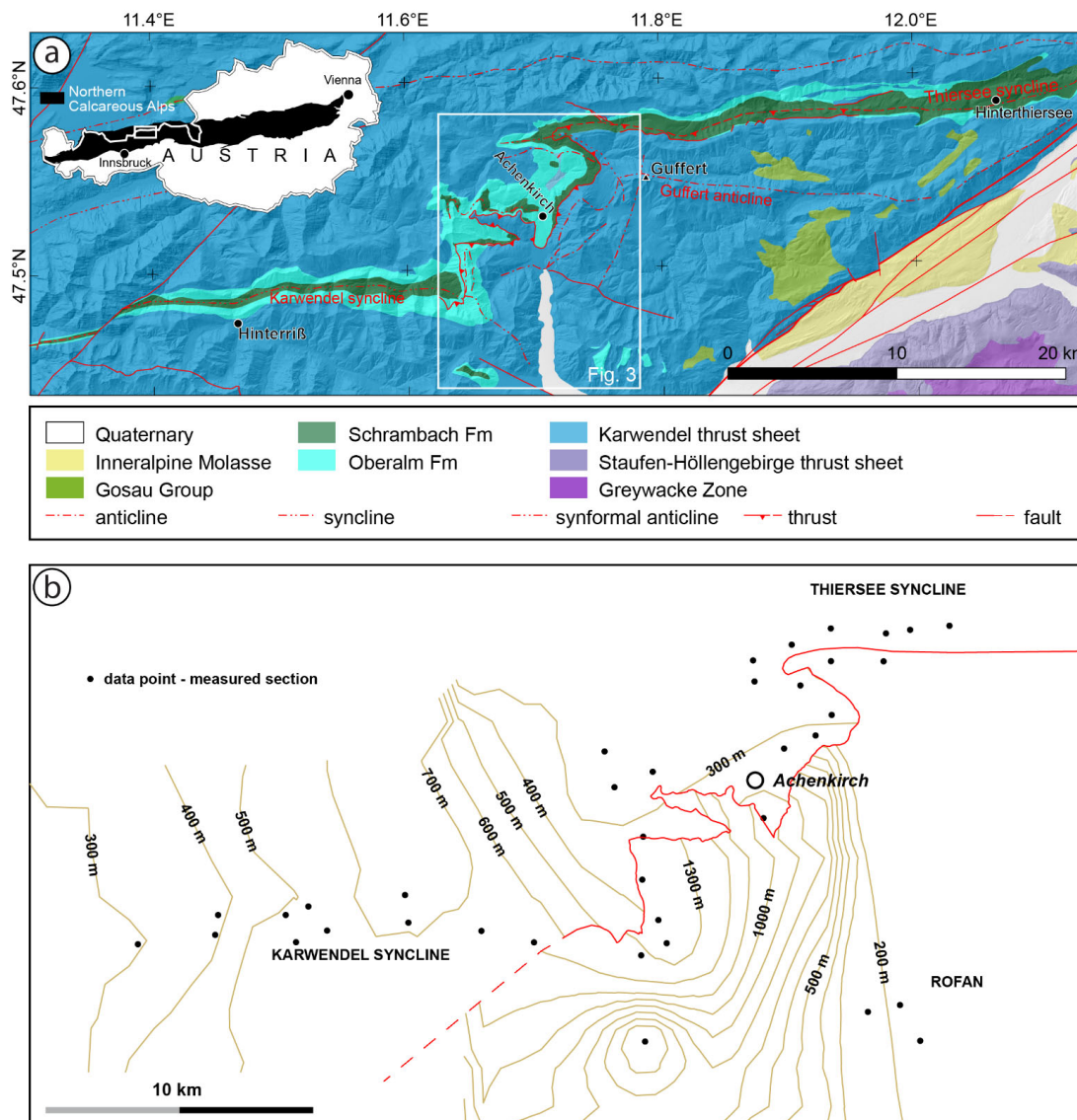
Figure 1: (a) Geological overview of the Achental structure within the Karwendel thrust sheet. Top inset shows the location of the NCA in Austria. Rectangle shows location of Figure 3. Modified after Ortner and Kilian (2016). (b) Isopach map of the Upper Jurassic Oberalm Fm. The Achental thrust (red line) is given for reference of location. Data compiled from Nagel et al. (1976) and Schütz (1979). Hanging wall and footwall of the thrust were contoured separately, single outliers in the data were ignored. Major thickness changes occur from W to E, a maximum is observed in the southern hanging wall of the thrust.

2.1 Sedimentary succession

The sedimentary succession of the NCA encompasses a late Permian to Early Cretaceous stratigraphic column that reflects the growth of two major Middle and Upper Triassic carbonate platforms and their subsequent drowning (Figure 2). During the Permian-Middle Triassic, the marine ingression of the Tethys led to the formation of a subtidal-supratidal marine environment, where evaporitic deposits (Haselgebirge) accumulated. The large amounts of halite, gypsum and anhydrite contained within these strata (Leitner and Neubauer 2011) are the cause of their highly incompetent behavior. The thickness of Haselgebirge is highly variable, due to salt diapirism and tectonics, although a primary thickness of 500-1000 m can be expected (Spötl 1989:

Fig. 2). Lower Triassic sandstones (Alpine Buntsandstein) overlie the Haselgebirge and are followed by the Anisian Reichenhall Formation (Fm) (Figure 2). The latter consists of alternating layered dolomite, cellular dolomite and bituminous limestone with a thickness of 80-200 m in the Achensee region (Nagel et al. 1976). The Haselgebirge-Reichenhall succession

110 composes a rheologically incompetent part of the stratigraphic column, forming the principal décollement of the NCA (Eisbacher and Brandner 1995). The Eben thrust (Figure 3) brings the Haselgebirge-Reichenhall succession to the surface in the Achensee region. Furthermore, its presence in the subsurface has been inferred from depth-extrapolated cross sections based on TRANSALP and industry reflection seismic lines (Auer and Eisbacher 2003: their Figure 15).

The evaporitic Haselgebirge-Reichenhall succession transitions into a succession of Anisian-Ladinian limestones (Alpine

115 Muschelkalk Group) (Bechstädt and Mostler 1974). These vary from shallow-water, strongly bioturbated mud- to wackestones (e.g., Virgloria Fm, Steinalm Fm) to basin marginal and basinal limestones (Reifling Fm) (Rüffer and Zühlke 1995). The uppermost Alpine Muschelkalk Group interfingers with the Wetterstein limestone (Anisian–Carnian), which forms the first of two major carbonate platforms of the NCA (Figure 2). Lithotypes consist of lagoonal, reefal and forereefal lime- and dolostones with a fossiliferous content of e.g., stromatolithes, oolites, calcareous algae and sponges; (Sausgruber 1994a) and their

120 fragments. Although the Alpine Muschelkalk Group and Wetterstein limestone show a general thickness between 1000 to >2200 m in the Achensee region (Sausgruber 1994b; Nagel et al. 1976; Gruber et al. 2022), cross sections in Gruber et al. (2022) show a thickness up to 3500 m. These thickness variations are attributed to salt tectonics in the Triassic (see Ortner and Kilian 2022; Granado et al. 2019; Kilian et al. 2021). The Carnian Raibl event marks the abrupt termination of carbonate sedimentation on the Wetterstein platform (Hornung et al. 2007; Krainer et al. 2011). As a result, the Raibl beds (Carnian)

125 overlie the Wetterstein platform unconformably. They consist of sandstones, shales, dolomites, cellular dolomites, evaporites and limestones that were deposited on a marine shallow shelf with interval-bound terrigenous input (Gruber et al. 2022; Krainer et al. 2011; Sausgruber 1994a; Jerz 1966). Compared to the underlying Middle Triassic carbonate platform, the Raibl beds form a relatively incompetent succession. The increased eradication of ripple marks and intercalated shale horizons marks the transition between the Raibl beds and the overlying Hauptdolomit carbonate platform (Müller-Jungbluth 1968: Fig. 2), forming

130 the second major platform of the NCA. Lithologies consist of inter- to supratidal, laminated dolostone and subtidal dolo-mudstones (Fruth and Scherreiks 1982; Müller-Jungbluth 1968; Zorlu 2007), which contain scarce fossils. The early evolution of the Hauptdolomit platform is characterized by local anoxic basins, represented in the stratigraphic succession by bituminous intervals and coaly shales (Spieler and Brandner 1989; Donofrio et al. 2003). Sedimentary textures typical for a supra- to intertidal lagoonal depositional environment (Flügel 2010) occur in the middle level of Hauptdolomit (Müller-Jungbluth 1968).

135 The Hauptdolomit platform subsequently drowns towards its top; the alternation of limestone and dolomite in the upper Hauptdolomit succession gradually evolves into the well-bedded and fossiliferous Plattenkalk limestone (Norian) (Gümbel 1861). Together, Hauptdolomit and Plattenkalk show a thickness > 1000 m in the Achensee region (Gruber et al. 2022; Nagel et al. 1976; Bachmann and Müller 1981; Sausgruber 1994a, 1994b). Further drowning resulted in the deposition of the subtidal Kössen Fm (Norian-Rhaetian) (Müller-Jungbluth 1968; Czurda and Nicklas 1971), marked by increasing intercalated marls

140 and shales (Lotter and Gruber 2011), which interfinger with Upper Rhaetian platform carbonates (Riedel 1988; Golebiowski 1991) (Figure 2).

While rifting of the Alpine Tethys (Eberli et al. 1993) in the Jurassic caused subsidence and drowning of the Triassic carbonate platforms (Ortner et al. 2008), rotational block faulting caused by the extensional movement (Lackschewitz et al. 1991) resulted in a differentiation of basin and swell facies (Nagel et al. 1976; Spieler and Brandner 1989). Early Jurassic red condensed

145 limestones (e.g., Adnet Fm, Sinemurian–Toarcian; Hierlatzkalk) containing manganese nodules (Sausgruber 1994a; Spieler 1994) were deposited on swells, and basinal strata (e.g., Scheibelberg Fm., Hettangian–Toarcian; Allgäu Fm. Hettangian–Oxfordian) in subsided areas (Brandner and Gruber 2011: Fig. 15). Gravitational scarp-fault breccias and debris flows are intercalated in the basinal slope specular limestones of the Scheibelberg Fm and the interfingering, more distal Allgäu Fm

(Spieler and Brandner 1989). The local basin-and-swell differentiation and sedimentation was preserved until the Middle-Late
150 Jurassic (Brandner and Gruber 2011; Ortner et al. 2008; Ortner and Kilian 2016; Spieler and Brandner 1989). The continental margin reached its maximum subsidence in the Oxfordian (Ortner and Kilian 2016), when the Ruhpolding radiolarite (Oxfordian) (Nagel et al. 1976; Sausgruber 1994a) as one of the deepest lithofacies of the Tethys (Bernoulli and Jenkyns 1974, p. 141) was deposited. The overlying Late Jurassic-Early Cretaceous (Kimmeridgian-Berriasian) stratigraphic succession (e.g., Tauglboden Fm, Ammergau Fm, Oberalm Fm, Barmstein limestones) testifies to a shallowing depositional environment
155 (Gruber et al. 2022; Gawlick 2004; Kilian 2013; Sausgruber 1994a; Gümbel 1861; Lipold 1854). The Jurassic succession (Scheibelberg Fm-Tauglboden Fm) has a mean thickness of 290 m (based on cross sections and compilations of Ortner and Gruber 2011; Sausgruber 1994b; Spieler 1995; Auer 2001; Gruber 2011). The Ammergau Fm (Kimmeridgian-Tithonian) has a mean thickness of 309 m and the Oberalm Fm (Tithonian-Berriasian) has a mean thickness of 1075 m.

An increase in siliciclastic detritus, beginning in the Early Cretaceous, marks the onset of synorogenic sedimentation,
160 commencing with the Schrambach Fm (Berriasian-Aptian), consisting of marls and intercalated calcareous and turbiditic sandstones (Lipold 1854; Ortner 2003a). In the western Thiersee syncline, its thickness is ~ 300-400 m (Ortner and Gruber 2011; Schütz 1979), thinning to ~ 150 m east of Achenkirch (Ortner and Gruber 2011). The overlying synorogenic sediments of the Gosau Group (Late Cretaceous to Paleogene) complete the stratigraphic succession of the Achental structure and Northern Calcareous Alps (Ortner 2003a).
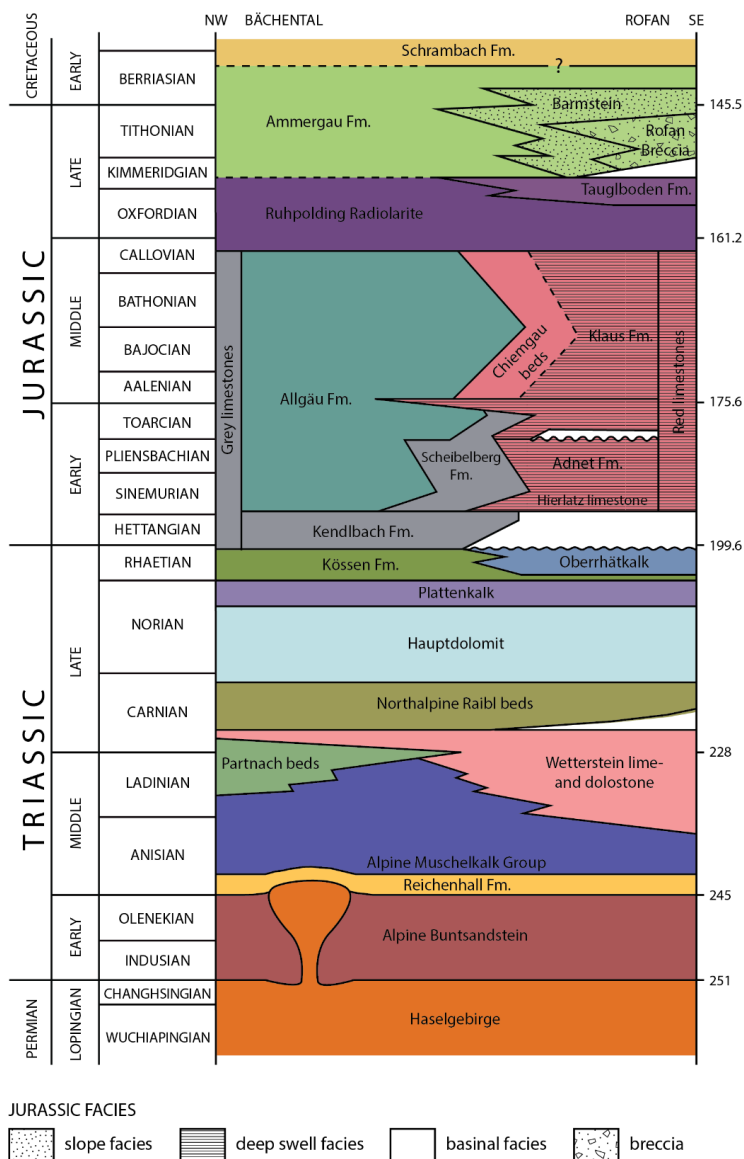
165

Figure 2: Stratigraphic overview of the Permian–Cretaceous sedimentary succession of the Karwendel thrust sheet in the Achensee area. Compilation of data from Piller et al. (2004), Nittel (2006) and Brandner and Gruber (2011).

2.2 Achental structure

The Achental structure is located within the Karwendel thrust sheet of the NCA and geographically surrounds Lake Achen

170 (German: Achensee) in Tyrol, Austria (Figure 1a, 3). The structure is characterized by the low-angle Achental thrust, which separates the Karwendel and Thiersee synclines in its footwall, from the Guffert-Unnutz-Montscheinspitze anticline fold train in its hanging wall. The Achental structure forms a NNE-SSW striking transfer zone between Karwendel and Thiersee synclines, with the Achental thrust reaching into the cores of these folds and gradually losing offset toward the NE and SW (Ortner and Gruber 2011). The thrust changes its orientation and stratigraphic offset throughout the Achental structure; in the

175 north (Mahmooskopf-Natterwand section, Figure 3), the thrust strikes E-W and dips ~ 23-30° south (Ortner 2003a and Beer 2003, respectively) with a total displacement of ~ 5-7 km (Auer and Eisbacher 2003 and Ortner 2003a, respectively). In the

central section, the thrust strikes NNE-SSW and dips 15° SE (Spieler 1994). It reaches a maximum stratigraphic offset of ~ 8 km (Eisbacher and Brandner 1996) NE of Achenkirch, where Hauptdolomit (Norian) is thrusted onto Schrambach Fm (Early Cretaceous) (Figure 3, 4a) (Gruber et al. 2022). In the south, the Achental thrust runs into the core of the Karwendel syncline

180 (Figure 3). Although here the thrust separates consecutive Late-Jurassic-Early Cretaceous strata, the SE dip of the thrust is strongly opposed to the steep E- to SE dip of the strata, ruling out a stratigraphic contact between these formations (Ortner and Gruber 2011). The Karwendel, Scharfreuter, Gröben and Großzemmalm synclines and the associated Hofjoch anticline and Klammbach syncline form the footwall of the Achental thrust (Figure 3). These are km-scale, E-W striking north-vergent folds that are overturned to recumbent, and are overridden by the Achental thrust and its associated faults (e.g., Leiten thrust; Ortner

185 and Gruber 2011: their Figure 2). The recumbent Thiersee syncline forms the north vergent eastern continuation of the Klammbach syncline (Ortner and Gruber 2011; Sausgruber 1994b; Gruber et al. 2022).

The hanging wall of the Achental thrust is referred to as the "Achentaler Schubmasse" after Quenstedt (1933). It is comprised of the connected Montscheinspitze, Unnutz and Guffert anticlines (Figure 3, 4), which change strike approximately parallel to the Achental thrust. West of the Achental structure, the Montscheinspitze anticline is connected to the Karwendel syncline

190 (Ampferer and Heissel 1950: their section 3). In the SW corner of the Achental structure, the northern anticline limb is folded with the Seebergspitze syncline into an overturned position (Fuchs 1944; Ortner and Gruber 2011) and thrusted onto the Karwendel syncline along the Achental thrust (Nagel et al. 1976). The Montscheinspitze anticline then continues toward the north as the Unnutz anticline, which is a recumbent fold with a SE-dipping axial surface and an increasingly SSW-plunging fold axis (From N-S 205/18, 200/27 and 187/23; Ortner and Gruber 2011). The Unnutz anticline (Figure 4a) resembles a dome,

195 rather than a cylindrical fold (e.g., Mojsisovics 1871; Sausgruber 1994a, 1994b; Ortner and Gruber 2011) with an upright limb that changes strike from E-W to NE-SW. NE of Achenkirch, the Unnutz anticline is folded around the Steigwand anticline and Rotmöserkopf synform and continues as the E-W striking Guffert anticline (Gruber et al. 2022; Ortner and Gruber 2011) (Figure 3, 4b). The Guffert anticline has a S-dipping axial surface, sub-horizontal fold axis with ESE-WNW strike and shows an overturned northern limb.

200 The resulting Guffert-Unnutz-Montscheinspitze anticline fold train in the Achentaler Schubmasse forms a characteristic sigmoidal shape that has been noticed since the beginning of the 20th century (Ampferer 1902) and is one of the greatest complexities in geologic interpretation of the Achental structure. Over the past century, four principal hypotheses have been developed to explain the formation of this sigmoidal fold train (see also Ortner and Gruber 2011; Gruber et al. 2022). These include *1)* bending of an originally E-W striking anticline due to rotational movements, forming the N-S striking Unnutz

205 anticline as a central segment (e.g., Ampferer 1921; Auer 2001; Spengler 1953, 1956; Ampferer 1941); *2)* passive dragging of the central part of the structure, caused by a larger amount of shortening in the eastern part of the structure, compared to its western part (Nagel 1975); *3)* polyphase deformation, in which a former W-directed thrust (Achental thrust) was reactivated by N-directed thrusting (Fuchs 1944; Channell et al. 1992; Channell et al. 1990; Ortner 2003a; Spieler and Brandner 1989), and *4)* forced folding of the Guffert-Unnutz-Montscheinspitze fold train at the border of a carbonate platform, or along an

210 inverted Jurassic normal fault (Eisbacher and Brandner 1995, 1996; Ortner and Gruber 2011).

In accordance with the third hypothesis, the Achental structure has been affected by polyphase shortening (Fuchs 1944; Spieler and Brandner 1989; Ortner 2003a; Ortner and Gruber 2011), beginning in the Early Cretaceous with the formation of the Guffert anticline (Ortner and Gruber 2011). Barremian sediments below the Achental thrust indicate an Early Cretaceous maximum age of thrusting. Both the Achental and Leiten thrust are folded with the E-W striking Roßstand anticline, but not

215 with the parallel Scharfreuter anticline (Sausgruber 1994b; Ortner and Gruber 2011: their Fig. 2) (Figure 3). Folding of the Achentaler Schubmasse around these folds suggests that the Achental thrust is older than the general N-directed shortening (Spieler and Brandner 1989). The oldest contractional deformation in the area is indicated by an angular unconformity in both limbs of the Guffert anticline at the base of the Gosau Group 15 km east of the Achental structure (Ortner and Gruber 2011),

indicating Early Cretaceous growth of the anticline. Anticlines grow on top of décollements, and we speculate that the Achental
220   thrust was already active. However, since the oldest sediments covering both the hanging wall and footwall of the northern
Achental thrust belong to the Gosau Group, N-directed shortening must have occurred post-Gosau (Ortner 2003a), post-dating
the formation of the western Achental thrust. Cretaceous shortening is evident from NNW- to NW-directed movement along
the Achental thrust (Eisbacher and Brandner 1995, 1996), based on calcite fibre lineations (Sausgruber 1994a, 1994b). This
phase of shortening caused an initial uplift and tightening of the Unnutz-Achental structure and is responsible for NW-striking
225   high-angle dextral transfer faults, which segment the Unnutz anticline (Eisbacher and Brandner 1995, 1996). In contrast, Late
Cretaceous to Paleogene (80-30 Ma) NE-directed shortening superimposed existing folds and fault movement, reactivating
pre-existing NW-striking transfer faults and forming NW-plunging folds and NE-striking high-angle transfer faults (Eisbacher
and Brandner 1995). As a result, three major fold orientations are recognized in the Achensee region (Sausgruber 1994a).
Folds with NE-SW striking fold axes formed during NW-directed, pre-Gosau contraction. E-W striking fold axes formed
230   during N-directed shortening and NW-SE striking fold axes formed during NE-directed shortening. Neogene folds
superimpose older folding and can be found e.g., within the Thiersee syncline (Sausgruber 1994b). In general, fold interference
creates intriguing dome-and-basin structures that complicate the geological interpretation of the Achental structure. Although
polyphase deformation of the Achental structure is visible from field evidence, showing refolded faults and fold axes (e.g.,
Gruber et al. 2022; Ortner and Gruber 2011; Sausgruber 1994b), it has not been proven that two phases of deformation were
235   necessary to create the Achental structure (Gruber et al. 2022).

Following the fourth hypothesis, several studies propose a link between a Jurassic basin architecture and the present-day
sigmoidal form of the Achental structure, suggesting that the latter is the result of forced folding (Eisbacher and Brandner
1995, 1996; Ortner and Gruber 2011) that depended on pre-existing extensional structures rather than the exact direction of
shortening (Töchterle 2005). The existence of a controlling inherited Jurassic basin-and-swell topography is supported by a
240   clear facies differentiation and an increasing thickness of basinal Jurassic strata, from 100 m near Mittenwald (30 km W of the
study area) to 1100 m in the Bächental (10 km NW of the study area; e.g., Ulrich 1960; Nagel et al. 1976; Schütz 1979; Ortner
and Kilian 2016; Gruber et al. 2022) (Figure 1b), showing an increased subsidence toward the SE end of the Karwendel
syncline. The Jurassic extensional basin-and-swell topography was proposed to form the foundation of the present-day
Achental structure, in which a N-S to NE-SW striking pull-apart basin (Spieler and Brandner 1989; Ortner and Gruber 2011)
245   or negative flower structure (Sausgruber 1994b) was bordered by E-W striking sinistral strike-slip faults. This is supported by
Pliensbachian and Toarcian mass-flow sediments and scarp-breccias that are found near the basin slopes (Spieler and Brandner
1989).

Figure 3: Geological map of the Achental structure compiled from Sausgruber (1994b), Spieler (1995), Auer (2001), Gruber (2011) and own data. Modified after Ortner and Gruber (2011). Sections A-A' and B-B' are shown in Figure 4.
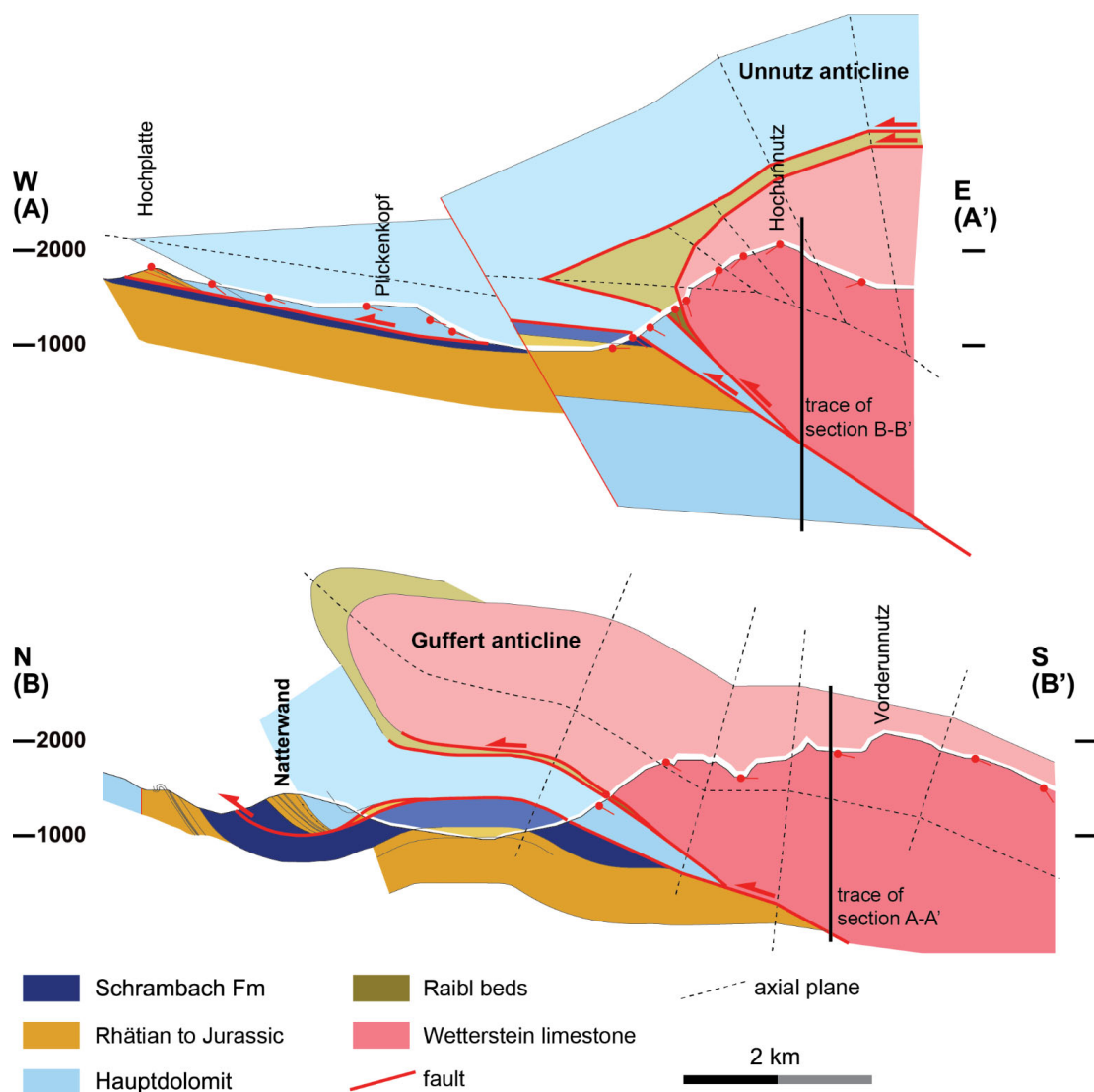
Figure 4: Cross sections (a) of the Unnutz anticline (Section A-A') and (b) of the Guffert anticline (Section B-B'). Section traces are marked in Figure 3. Modified after Ortner (2003a).

3 Analogue modelling

3.1 Modelling strategy

Regional-scale physical analogue modelling was conducted to investigate the influence of pre-existing basin-bounding extensional faults on oblique basin inversion, within the geological framework of the Achental structure. The goals of the experiments included testing 1) the importance of a weak basal décollement, 2) the influence of thick-skinned versus thin-skinned tectonics, and 3) the role of pre-existing structures in deformation localisation. Analogue models were set up to show an increasing lithological and structural likeness to the eastern margin of the Jurassic Achental basin, resulting in an increasing model complexity.
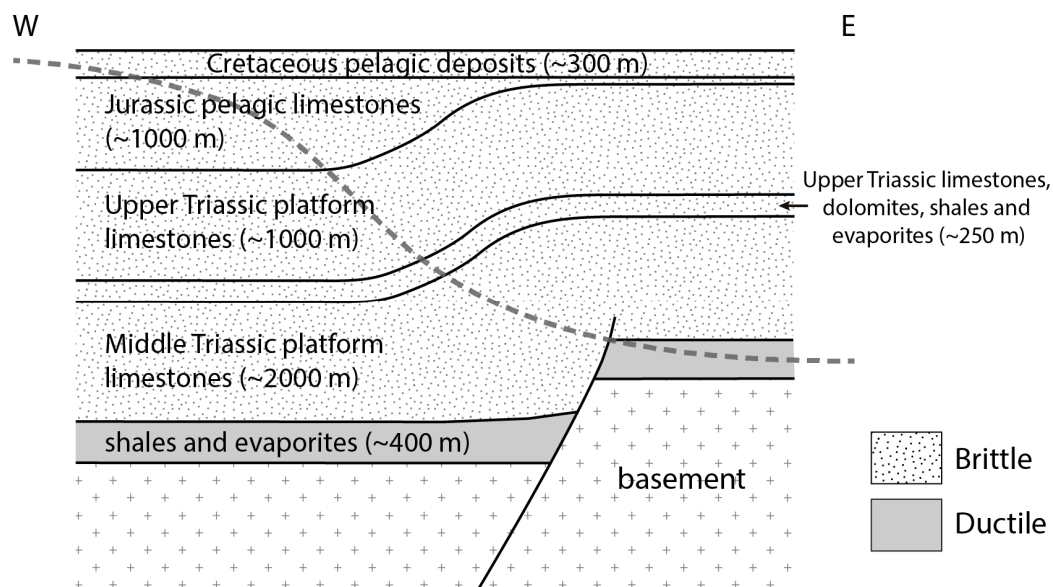
Figure 5: Schematic diagram showing the geological set-up of the eastern margin of the Achental basin, prior to inversion. Grey bold line represents inversional trace of the Achental thrust. Lithologies are marked brittle or ductile, depending on their mechanical properties.

3.2 Geometric and kinematic setup

265

Brittle and ductile modelling materials represent different parts of the NCA and Tethyan stratigraphy. A ductile layer of ~ 400 m thick, incompetent evaporites and shales, forming the basal décollement of the NCA was represented by silicone putty in models, with a thickness of 0.4 cm (Figure 5 and 6a). The silicone putty is a mixture of RBG-0910 Dow Corning silicon polymer and fine iron powder (~ 32 wt.%) with a density of ~ 1360 kg m^{-3}. We determined a viscosity (η) of 20456 Pa s for

270 the modified silicone putty, using a coni-cylindrical viscometer under room temperature (21 ± 1 °C) (Mooney and Ewart 1934; Lee and Warren 1940, see also Willingshofer et al. 2005). The viscosity of natural evaporites, albeit highly variable, is estimated to be 10^{19} Pa s (Allen and Beaumont 2016; Weijermars 1986a; Weijermars 1986b, 1986c; Weijermars et al. 1993; Weijermars and Schmeling 1986), resulting in a viscosity ratio of $2.046 \cdot 10^{-15}$. The modified silicone putty exhibits near-Newtonian behaviour and has an n-value of 1.27 in laboratory tests. The predominantly carbonatic, brittle sedimentary cover

275 of the NCA was represented by dry quartz sand (Figure 5), a Mohr-Coulomb material, with a density of 1510 kg m^{-3} (e.g., Willingshofer et al. 2018). The quartz sand was sieved on top of the silicone putty, to create a total model thickness of 5 cm (Figure 6a). The density of the natural prototype was approximated by the density of Triassic Muschelkalk and amounts to ~ 2680 kg m^{-3} (Manger 1963: p. E31), so that a density ratio (ρ*) of 0.56 between model and nature exists. An intermediate layer of Upper Triassic carbonatic-evaporitic strata was modelled as either brittle or ductile, depending on the model-specific set-

280 up (Figure 6a, 6b). Assuming that inertial forces can be neglected in the analogue models (see discussion in Wickham 2007; Del Ventisette et al. 2007), the scaling of time and length is allowed to deviate from the principle of dynamic similary and their "ratios can be considered as independent variables" (Dombrádi et al. 2010, p. 109). The principles of dynamic, geometric and rheological scaling are discussed in Hubbert (1937), Ramberg (1981), Weijermars and Schmeling (1986), Merle and Abidi (1995), Brun (1999), Sokoutis et al. (2000; 2005) while their relationships between model and nature are summarized in Table

285 1.

Table 1: Summary of model parameters. Experimental material parameters from Willingshofer et al. (2005; 2018). For strength envelops, see Figure 6b.

Materials/parameters		Model	Nature	Ratio (m/n)
Brittle layer	Thickness	Max. 0.05 m	Max. 5000 m	10^{-5}
(Quartz sand)	Density	1510 kg m^{-3}	2680 kg m^{-3}	0.56
	Strength	Max. 1471.5 Pa	Max. $2.63 \cdot 10^{-8}$ Pa	$5.597 \cdot 10^{-6}$
Ductile layer	Thickness	0.004 cm	400 m	10^{-5}
(Silicone mixture)	Density	1360 kg m^{-3}	2450 kg m^{-3}	0.56
	Viscosity	20456 Pa s	10^{19} Pa s	$2.046 \cdot 10^{-15}$
	Strength	28.41 Pa	2550933 Pa	$1.11 \cdot 10^{-5}$
	n-value	1.27		
Length				10^{-5}
Strain rate		0.01 m/h	0.00323 m/yr	27137
Time		8–11 h	2.478–3.408 Ma	$3.685 \cdot 10^{-10}$
Bulk shortening		0.08–0.11 cm	8000–11000 m	10^{-5}

Model materials were placed in a rectangular fault box with metal bars as sidewalls and a wooden piston of 40 or 83 cm width

290 as a moving wall (Figure 6c). We chose a length ratio (L*) of 10^{-5}, so that 1 cm in the model represents 1 km in nature (Table 1). In all experiments, a pre-existing normal fault, similar to the boundary fault of the Achental basin was represented by a rigid basal plate (footwall block) with a 60° dipping ramp (fault plane). In model-specific set-ups, the direction of shortening (at 90 or 45° to the ramp), the movement of the basal plate (fixed or mobile) and the layering sequence of the model (Figure 6a) were varied. The modelling strategy evolved from a basic model set-up, which was applied to one brittle (A1) and three

295 brittle-ductile (B1-3) models. The set-up featured a basal plate with dimensions of 40 x 22.5 cm, a thickness of 1 cm and a 60° dipping front ramp (Figure 6). A wooden piston of 40 cm width was placed behind (A1, B1) or on top of (B2, B3) the basal plate, so that the plate was either mobile or fixed, exemplifying the effect of thick- versus thin-skinned tectonics. Shortening was applied at 90° to the front ramp with a convergence rate of 8 cm/h for the brittle model (A1) and 1 cm/h for the brittle-ductile models (B1-B3), and a total shortening of 8 cm (Table 1). For the brittle model, only quartz sand was used as a

300 modelling material. In the brittle-ductile models, a basal layer of silicone putty was placed on top of the basal plate (B1, B3) or over the basal plate, ramp and tabletop (B2). A small amount of dishwashing soap was spread between the plate and the silicone putty, to increase the décollement function of the ductile layer. Model B2 featured an additional, upper ductile layer (Figure 6a). For model C1 we added two plates to the north and south of the fixed main basal plate, to simulate E-W striking strike-slip faults bounding the Achental basin. This required the use of a piston with a width of 83 cm. Shortening remained

305 orthogonal to the ramp at 1 cm/h, but total shortening was increased to 11 cm. The basal ductile layer of silicone putty was placed on top of the basal plates and on the tabletop, but was disconnected at the ramp (Figure 6). For models D1 and D2 the fixed main basal plate and two auxiliary plates were rotated 45°, to simulate oblique shortening at 45° to the ramp. We applied a total shortening of 11 cm. For both models, the basal ductile layer was placed on the basal plate and tabletop, while being disconnected at the ramp to create a clear velocity discontinuity (see e.g., Allemand and Brun 1991; Tron and Brun 1991), but

310 model D2 featured an extra, upper ductile layer. After reaching the desired shortening, models were covered with black sand for protection, drenched with water until saturation and left to rest for at least 2 hours. Sections were then cut orthogonal to the strike of major structures.
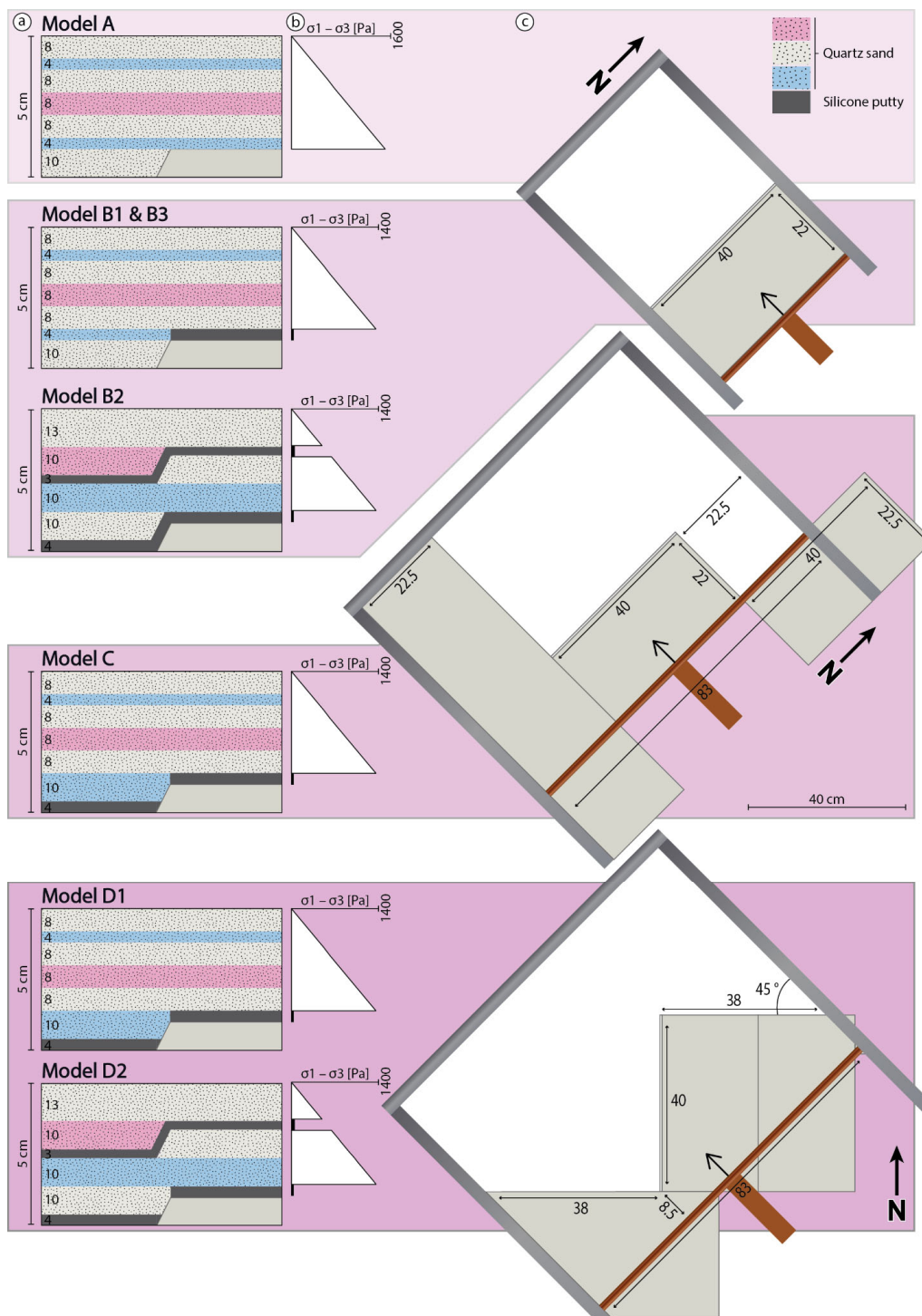
Figure 6: Modelling set-up for model series A-D. (a) Layering sequences showing differently coloured layers of quartz sand and silicone putty with a total thickness of 5 cm. (b) Strength envelops showing strength (in Pa) of different modelling materials. (c) Basal plate set-ups showing the basal plate size (in cm).

3.3 Monitoring and model analysis

Particle image velocimetry (PIV) was used to analyse incremental displacements in the analogue models (see e.g., Leever et al. 2011; van Gelder et al. 2017), using powdered coffee grains on the model surface as markers. For all models, photographs

320   of the top surface of the experiment were taken in a fixed time interval of 30 minutes. Photos were then rectified to correct for lens distortion and processed using the MATLAB® vR2022a application PIVlab v2.57 (Thielicke and Sonntag 2021; Thielicke and Stamhuis 2014; Thielicke 2014). In the image pre-processing settings, we enabled Contrast-Limited Adaptive Histogram Equalization (CLAHE) to locally enhance the contrast. FFT window deformation was used as the PIV algorithm. As post-processing steps we applied a vector validation using a standard deviation filter and interpolated missing data points.

325   The "strainmap" package (Broerse 2021) for MATLAB® (vR2022a) was used for calculating cumulative strain type maps for models C and D1 based on incremental displacements from the PIV analyses. For a review of the underlying algorithms and practical applications of this software, see Broerse et al. (2021) and Krstekanić et al. (2021; 2022). Resulting colour-coded maps show the cumulative strain type (extension, strike-slip movement or shortening) at four points during the model runs (see figures in Sect. 4).

330   ### 3.4 Limitations and simplifications

One of the major limitations of the experiments in this study is the necessary simplification of the initial fault configuration. The Jurassic basin-bounding faults are presently not exposed at the surface and thus their geometry and exact position are not known. It is assumed that the major present-day structural elements are aligned to the margins of the Jurassic Achental basin (Sausgruber 1994b; Töchterle 2005; Ortner and Gruber 2011). Therefore, a simple initial fault arrangement with one N-S and

335   two E-W striking elements was chosen as the basis for the analogue models. Splay faults and additional basin-bounding faults are thus not considered here. The models were shortened in one single phase, simulating Cretaceous NW-directed shortening. However, the Achental structure was affected also by N-directed Paleogene and NE-directed Neogene shortening (Eisbacher and Brandner 1995; Ortner and Gruber 2011). These posterior phases of deformation were not taken into consideration for the analogue modelling, because they cannot explain the large offset along the Achental thrust in W–E sections (Ortner and Gruber

340   2011; Ortner 2003a) and are thus not expected to have created the main structural elements. The model set-up emphasizes the rheological contrast between a weak ductile basal décollement and a stronger upper brittle layer, whereas the characteristic, more complex heterogeneity of the NCA sedimentary cover was not included. Finally, the models ignore natural recovery processes such as erosion and sedimentation, which may influence the time–space evolution of structures. Despite these simplifications, our analogue models were able to tackle the problem and trace the large-scale deformation pattern as a response

345   to compression.

4 Results

Model A is a purely brittle experiment with a maximum thickness of the sand layer of 5 cm. The piston pushed both the sand and the basal plate. In the initial stages of the experiment, an asymmetrical pop-up structure with a master back-thrust (1) and an antithetic fore-thrust (1) formed (Figure 7). The master thrust is accompanied by a blind thrust that did not fully reach the

350   surface. Further shortening was accommodated by transient fore-thrusts (2, 6-8), which developed at the base of the ramp and migrated upward through the wedge, along the master thrust, with increasing shortening. At 50% of total shortening, the frontal part of the wedge experienced gravitational collapse along a normal fault (4).
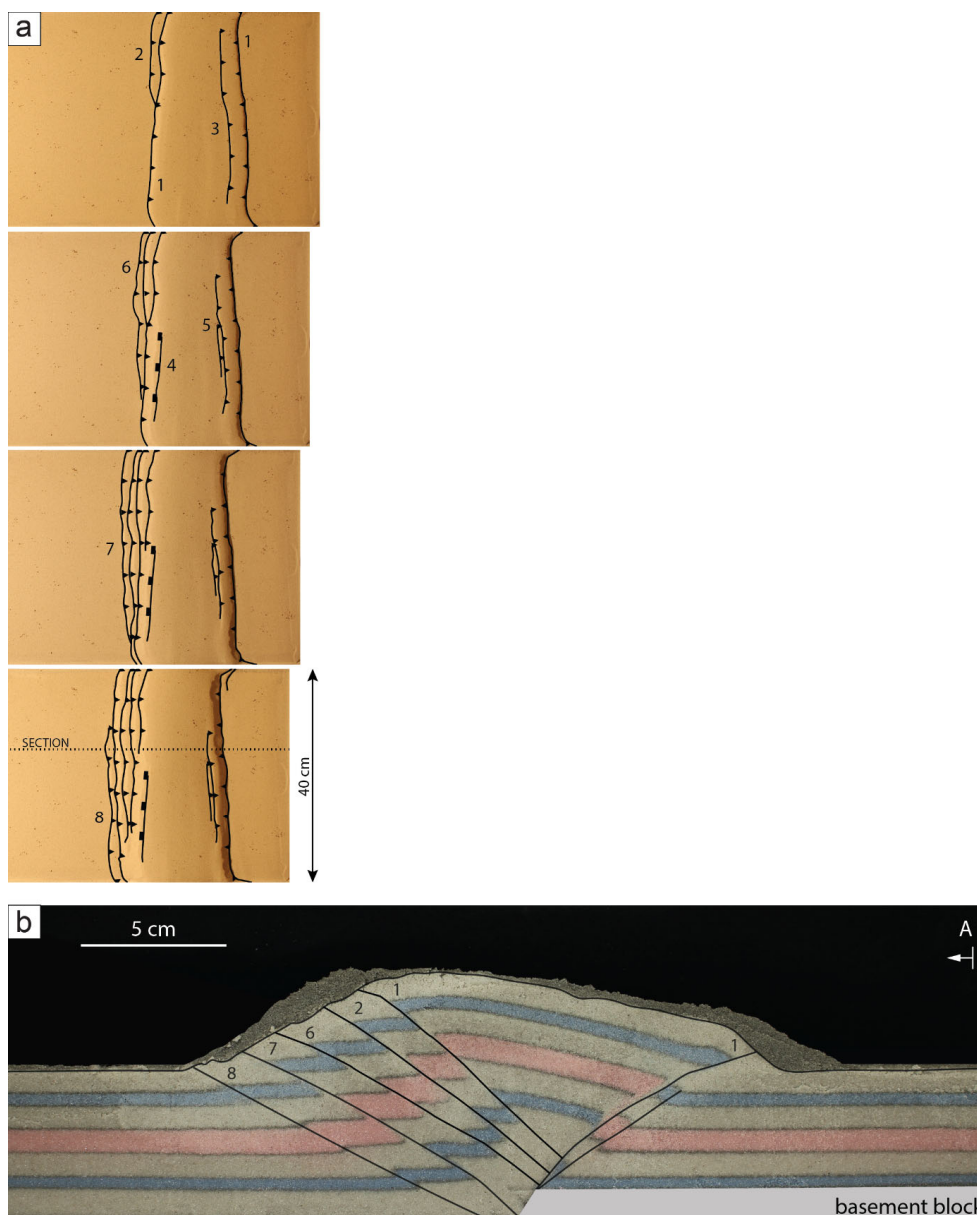
Figure 7: Modelling results of model A, showing (a) top views at 25, 50, 75 and 100 % of total shortening, and (b) side view at 100 % of total shortening. Location of section is marked in (a). Numbers show sequence of initial fault activity.

Model B1-B3 (Figures 8 and 9) were set up similar to model A, but were designed as brittle-ductile models with a basal detachment of silicone putty, to study coupling and decoupling processes at the basal plate and ramp. Model B1 initially developed an asymmetrical pop-up structure with an antithetic fore-thrust (1) and a master back-thrust (2) similar to model A (Figure 8a, 9a). Shortening was initially accommodated equally along the back-thrust and the fore-thrust, but final sections show that the bulk shortening occurred along the master back-thrust. With further shortening, additional fore-thrusts (7, 9) form and previously active thrusts migrate upward along the master back-thrust. All major thrusts originate from the velocity discontinuity at the ramp. Several secondary pop-up structures formed along splay faults (e.g., 3, 4, 6). The final resulting wedge is both wider and lower than in the brittle model A, and the internal wedge structure more complicated. In model B2,

we tested a different layering sequence with an additional, upper ductile layer. Furthermore, the basal ductile layer was draped
365   over the entire model base and connected at the mobile ramp, as opposed to model B1, where the silicone putty was placed
only on the basal plate (Figure 6a). During the first 25% of total shortening, a central wedge developed over the ramp, formed
by two main back-thrusts separated at the upper layer of silicone putty. Deformation shifted to the hinterland at ~50% of total
shortening, where an asymmetrical pop-up structure with a main back-thrust was formed in the lower sand layers, and a
symmetrical pop-up structure was formed in the upper sand layer above the upper ductile horizon. Pockets, filled with air that
370   was trapped underneath the silicone during model construction and migrated during shortening, form modelling artefacts.
Overall, the height of the resulting wedge was far less than in model B1 and structures were mainly hinterland-oriented and
dominantly backwards thrusting (Figure 8b, 9b). Thrusts might have initially originated at the velocity discontinuity, but were
laterally transported onto the mobile basal plate as shortening progressed. The upper and lower sand layer were completely
decoupled at the upper silicone layer. For model B3 we used an identical layering as for model B1, but the basal plate was
375   fixed and the piston was placed on top of the basal plate (Figure 6). In the first half of the experiment (0-50% total shortening),
a flip-type pop-up structure (see Smit et al. 2003, their Figure 4) with two back-thrusts and conjugate fore-thrust (1) developed
directly in front of the piston (Figure 8c, 9c). Movement occurred along the main back-thrust, switched to the fore-thrust and
back to the secondary back-thrust, as visible from lobes of silicone putty along the thrusts. At ~ 75% of total shortening,
thrusting propagated into the foreland to form a strongly asymmetric pop-up structure with a master fore-thrust (5) and a minor
380   back-thrust (6). The master thrust originated directly at the velocity discontinuity above the ramp. Although in the fixed plate
scenario, as opposed to the mobile plate scenario, deformation did not localise directly above the ramp but rather required a
wedge in the hinterland, the wedge geometry is much more asymmetric with most of the shortening occurring along a low-
angle master fore-thrust that is antithetic to the original normal fault geometry.
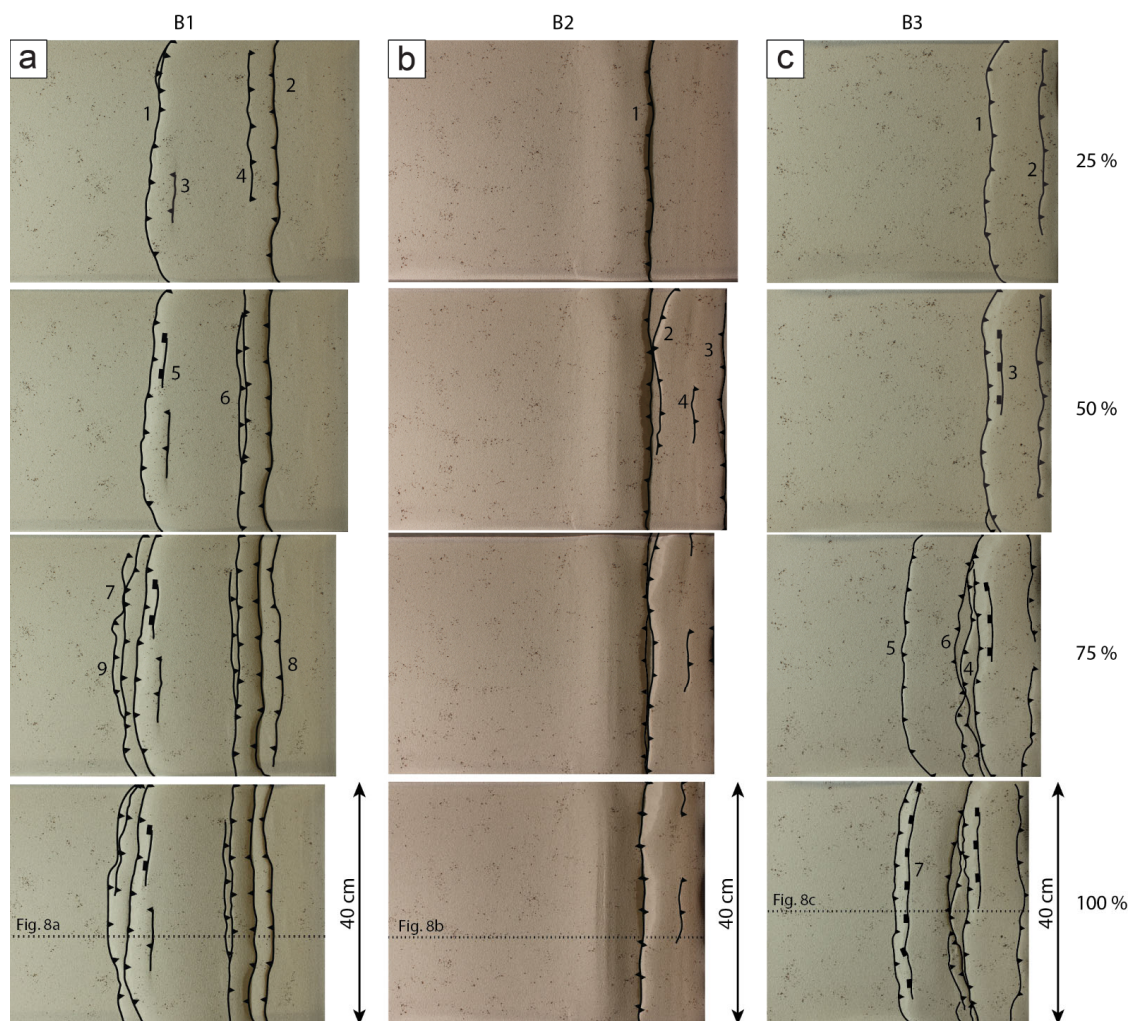
385 **Figure 8:** Top views of models (a) B1, (b) B2, and (c) B3 at 25, 50, 75 and 100 % of total shortening. Locations of sections are indicated (dotted lines). Numbers show sequence of initial fault activity.
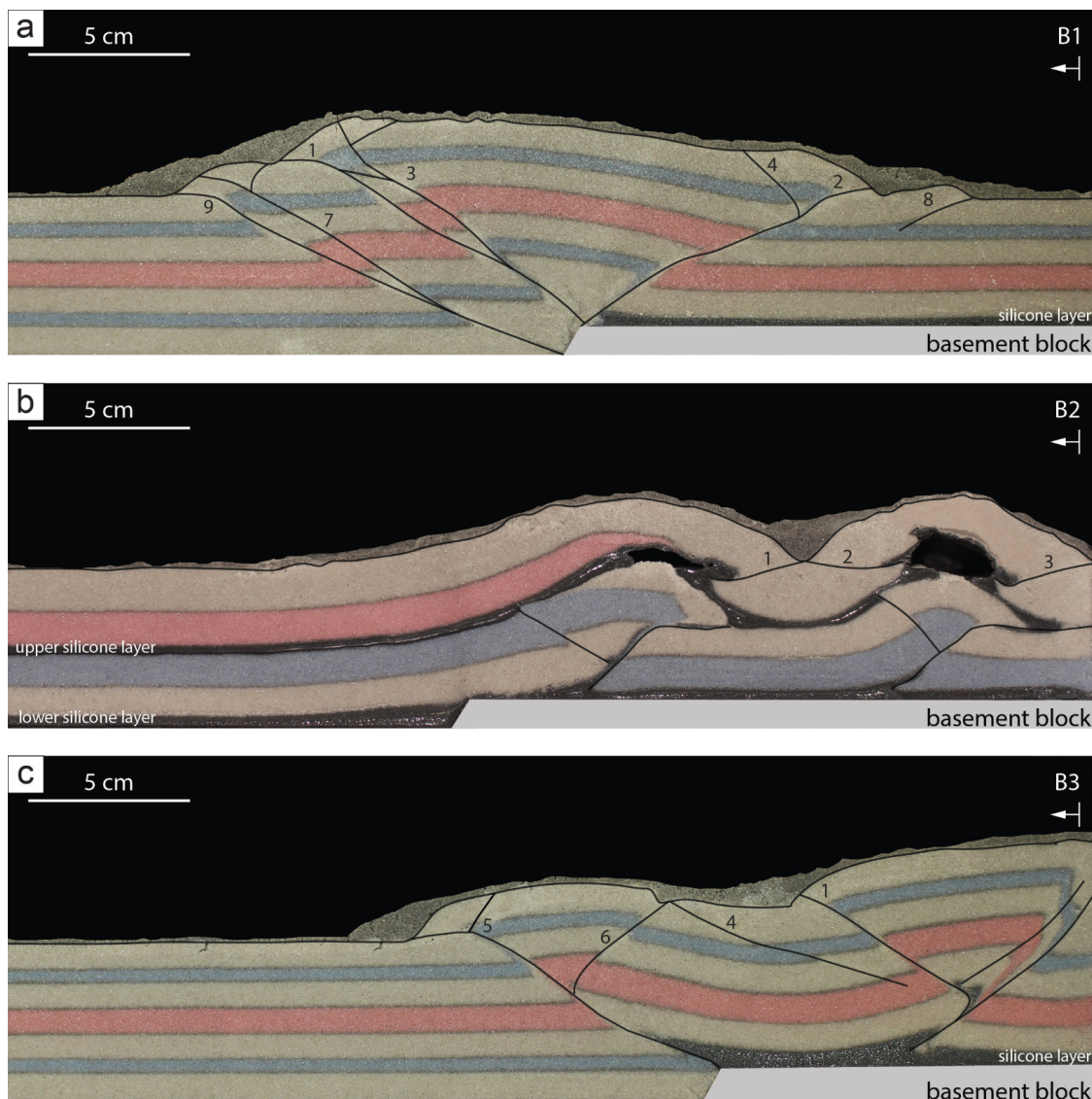
Figure 9: Side views of models (a) B1, (b) B2, and (c) B3 at 100 % of total shortening. Locations of sections are marked in Figure 8. Numbers show sequence of initial fault activity.

390 For model C, we increased the number of basal plates to three, aligning them so that the margins of the plates formed one N-S and two E-W striking elements (Figure 6c). We placed silicone putty on both the basal plates and the table top, disconnecting it at the ramp to form a similar mechanical scenario as in model B3. Because of the larger size of the model, we increased the total shortening to 11 cm. Initially, a slightly asymmetrical pop-up structure formed close to the piston, with a back-thrust that migrated slightly upward along the main fore-thrust (2) (Figure 10a, b). Additional fore-thrusts (1, 3) developed especially in

395 the northern area of the model, where the basal plate was missing. After approximately 55% of total shortening, deformation propagated into the foreland, where a second asymmetrical pop-up structure formed above and parallel to the ramp in the subsurface. The master fore-thrust (5) accommodated most of the shortening, whereas several minor back-thrusts migrated upward along the master thrust. The sand layer forms a ramp anticline over the master thrust, which approaches lower angles toward the surface. Close to reaching the total shortening, deformation propagated in the southern area of the model, where

400   the basal plate reaches into the foreland, and third pop-up structure was formed there (9), but was not able to develop further
with this amount of shortening. Overall, the wedge was relatively low compared to the brittle model A and the brittle-ductile
model B1. The deformation front at total shortening approximately shows the contours of the basal plate in the centre and
southern parts of the model (Figure 10a).

Calculation of mean shortening vectors via PIV analysis shows that surface deformation occurs in the tectonically active region
405   west of the deformation front, with a localisation of strain at the foremost thrust (2, 5, 9/10). Vectors rotate outward on both
the northern and southern side of the wedge. The dominant type of strain at the active fore-thrusts is shortening (red colours
in Figure 10c). Extensional strain on top of the wedge (blue colours in Figure 10c) is mainly caused by gravitational collapse
of parts of the wedge. More importantly, along the entire deformation front, strike-slip strain (turquoise colours in Figure 10c)
is subordinate to shortening, even in areas of the model where the trace of the deformation front is oblique to the direction of
410   shortening.

s
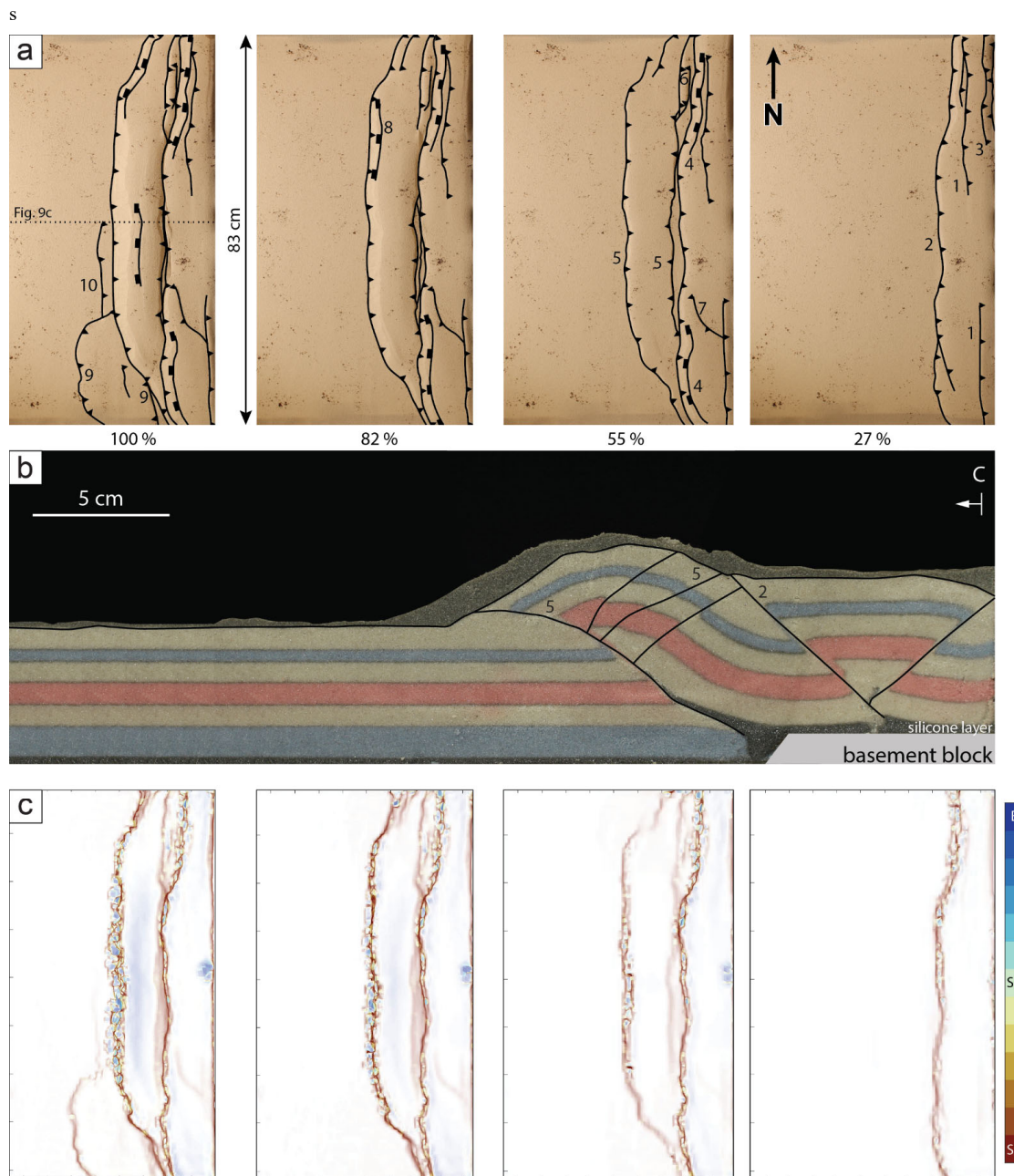
Figure 10: Modelling results of model C, showing (a) top views at 27, 55, 82 and 100 % of total shortening, and (b) side view at 100 % of total shortening. Numbers show sequence of initial fault activity. (c) Strain type analysis of model C, showing areas of extension (E), strike-slip movement (Ss) and shortening (Sh).

For model D1 and D2 the plate set-up was rotated, so that shortening was directed at an angle of 45° to the basal plate and ramp (Figure 6c). Model D1 used a layering sequence identical to model C. In the initial stages of the experiment, up to 55% of total shortening, a pop-up structure developed over the entire length of the piston (Figure 11a). In the south of the model, the initial pop-up structure is asymmetric with a main fore-thrust, whereas in the centre area of the model, where the basal plate set-up creates a 90° angle, the structure is of a flip-type (see Smit et al. 2003, their Figure 4), where shortening was

initially accommodated along a fore-thrust, before switching to a back-thrust. The structures did not form entirely parallel to the piston, but from approximately 27% of total shortening on, the wedge widened along the main fore-thrust (1) in the south, where the basal plate extends into the foreland, whereas in the centre and north of the model, shortening was accommodated by a series of minor fore-thrusts (3-5) that migrated along their associated back-thrust. The thrusts are more closely spaced within the corner between the plates. With further shortening, the wedge propagated, first on the southern basal plate (7) from approximately 82% of total shortening, and in a later stage on top of the northern plate (8). The surface expression of the propagating fore-thrusts runs parallel to the plate structure in the subsurface; whereas sections show that they originate directly at the velocity discontinuity at the ramp (Figure 12a, b). The fore-thrusts form hinterland-dipping (~30°) master thrusts in strongly asymmetric pop-up structures, similar to model B3. In contrast, in the corner between basal plates shortening is completely accommodated within the initial pop-up structure with a steepening of the back thrust, caused by the confinement of the piston, and irregularly spaced fore-thrusts that migrate, but do not propagate significantly. In all cases, deformation does not propagate further than the velocity discontinuity and thus stays within the upper décollement level.

PIV analysis of the incremental displacements shows that shortening localises at the foremost thrust in model D1 (1, 7). When analysing the strain type, the results are similar to model C, in the sense that shortening is the dominant type of strain, independent of the orientation of the thrust trace, whereas the dominant strain direction is mostly perpendicular to the thrust trace. As such, the orientation of the basal plates evidently controls the orientation of the thrusts, with a rotating local strain field, depending on the plate in the subsurface.

In model D2, the same basal plate set-up was used as in model D1, but we tested the effect of two ductile layers, similar to model B2 (Figure 6). Similar to model D1, an initial pop-up structure formed at the wedge, featuring a main back-thrust within the lower part of the model, which is decoupled from the upper part at the upper ductile layer. Propagation into the foreland occurred swiftly, beginning around 55% of total shortening, resulting in pop-up structures with a master fore-thrust in the lower sand layer, which localised at the ramp (Figure 11c, 12c). The pop-up structures form a sigmoidal shape that straddles the basal plate structure in the subsurface. However, due to the strong decoupling at the upper ductile layer, the surface structures do not reflect the situation in the lower part of the model and the wedge reached far less height than in experiments with a single ductile layer.
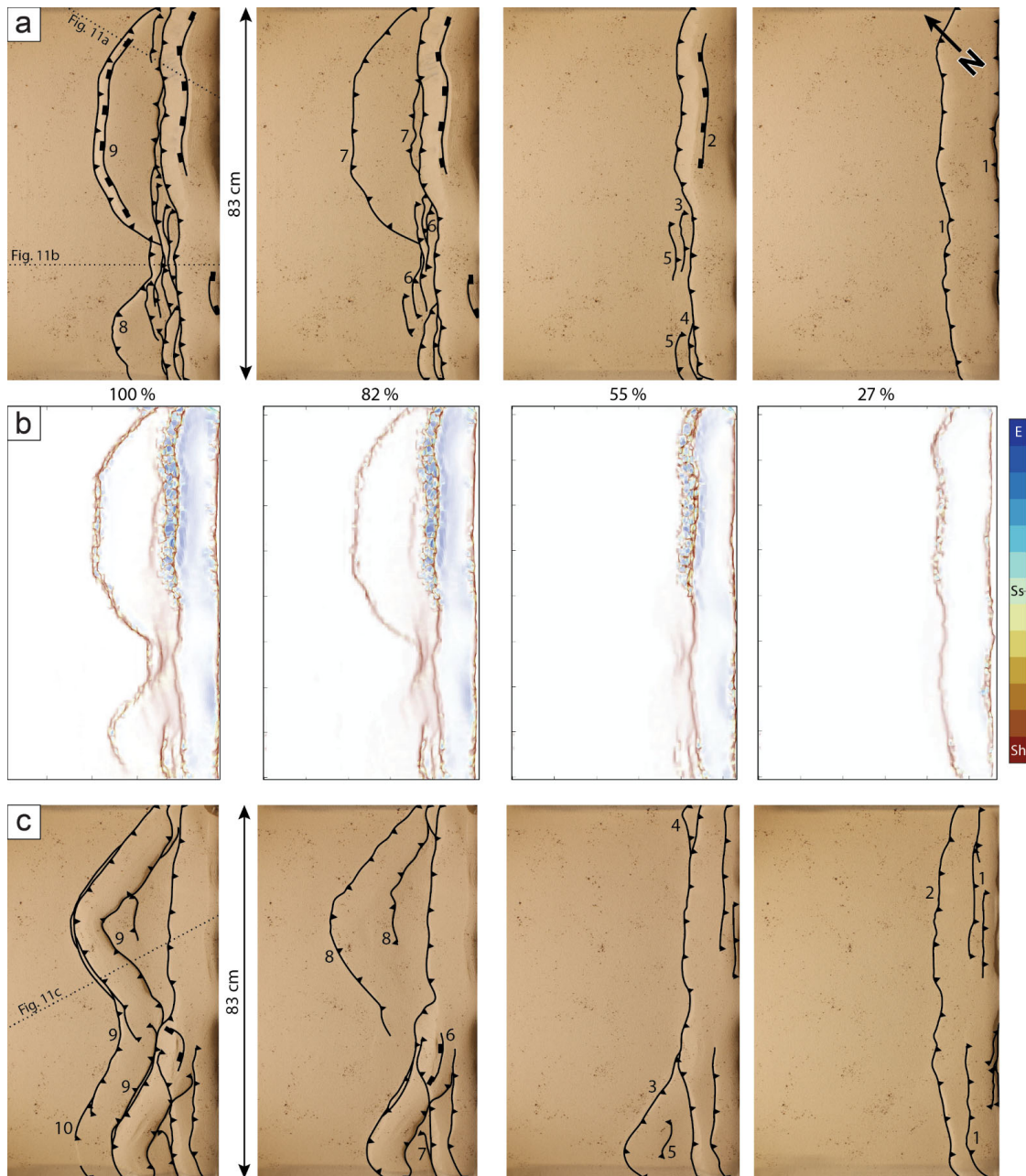
Figure 11: Top views of models (a) D1, and (c) D2 at 27, 55, 82 and 100 % of total shortening. Numbers show sequence of initial fault activity. PIV strain type analysis of model (b) D1, showing areas of extension (E), strike-slip movement (Ss) and shortening (Sh).
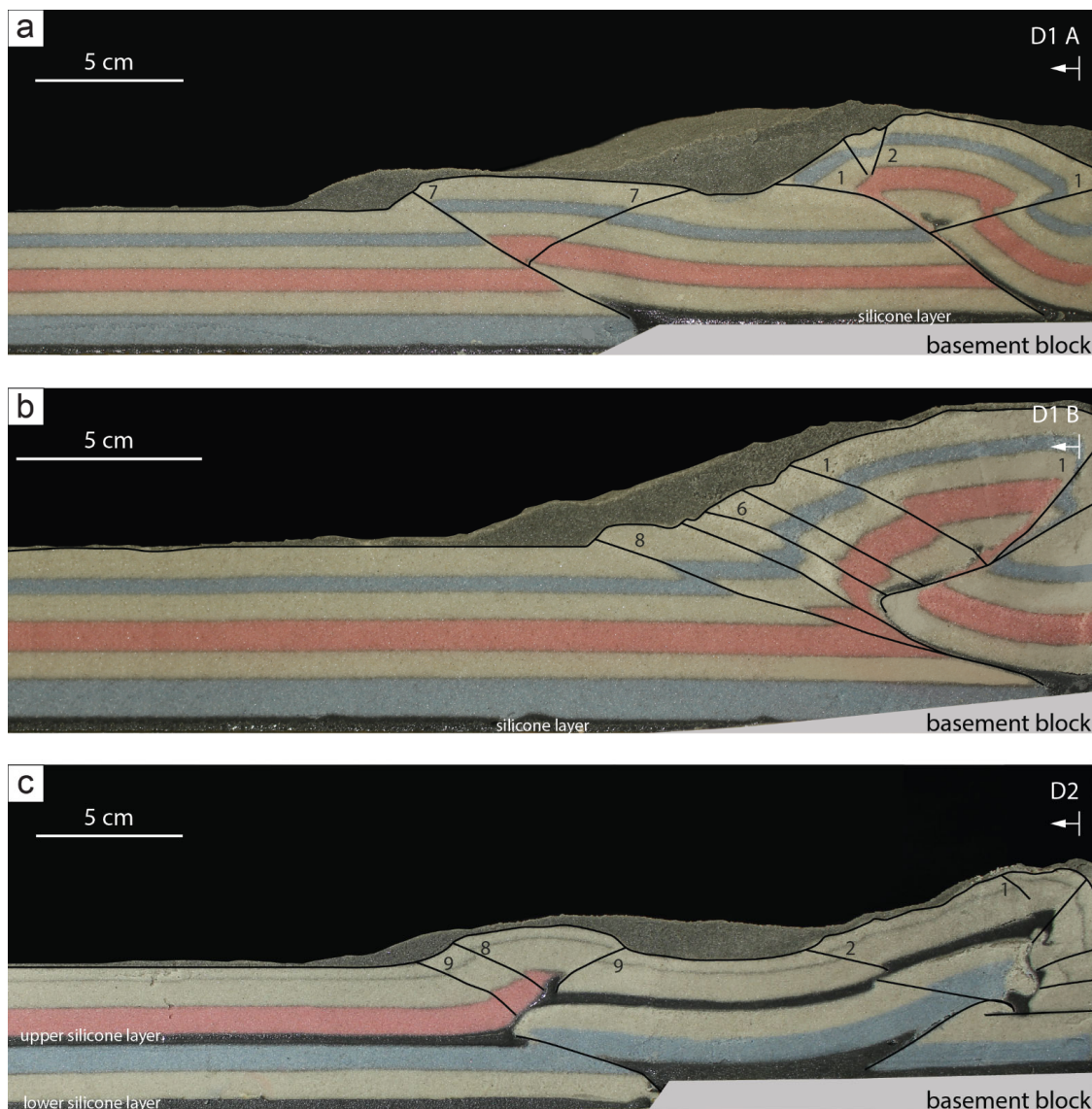
Figure 12: Side views of models (a, b) D1, and (c) D2 at 100 % of total shortening. Numbers show sequence of initial fault activity.

5 Discussion

5.1 Analogue modelling

455   Inversion of basins, either orthogonal or oblique to the former basin margins, has been subject of many analogue modelling studies (e.g., Deng et al. 2020; Yagupsky et al. 2008; Del Ventisette et al. 2006; Bonini et al. 2012; Brun and Nalpas 1996; Zwaan et al. 2022). The high variance of geological structures leads to a myriad of deformation styles characterizing inverted and reactivated fault systems (Bonini et al. 2012; their Figure 3), especially for inversional set-ups involving a viscous décollement (Brun and Nalpas 1996). The modelling strategy (see Sect. 3.1) followed in this study aimed to test three factors

460   that may affect the structural grain of obliquely inverted extensional basins. These factors included the influence of 1) a weak basal décollement, 2) pre-existing structures attributed to an extensional basin, and 3) thick-skinned or thin-skinned tectonics.

The increasing complexity of the models is a result of consecutively implementing parameters that were found to be of relevance to the natural example, the Achental structure. Apart from its sigmoidal hanging wall shape, one of the complexities of the Achental structure is that its dominant fore-thrust is antithetic to the existing Jurassic normal fault in the subsurface
465 (Figure 5). Most of the deformational styles associated with basin inversion are synthetic to existing normal faults (e.g., Héja et al. 2022: their Figure 4 and 11; Bonini et al. 2012: their Figure 3), although the formation of an antithetic low-angle thrust has been predicted (Laubscher 1986; Tavarnelli 1996) and successfully simulated (Caër 2016).

5.1.1 Influence of mechanical stratigraphy

In our study, the influence of a weak basal décollement has been tested using two models (A1 and B1). These have an identical
470 mechanical set-up, using a rigid ramp, which represents a pre-existing normal-fault controlled mechanical heterogeneity in the model and is pushed into a brittle (A1) or brittle-ductile (B1) cover. The brittle model shows strong similarities to existing analogue experiments (e.g., Bonini et al. 2000; Persson and Sokoutis 2002) and the brittle-ductile model (B1), but the latter shows a markedly lower angle of thrusting, wider thrust spacing and faster propagation. Decoupled thrust wedges are known to show these effects in analogue models, attributed to a lower basal friction compared to frictional Coulomb wedges (Smit
475 2005; Smit et al. 2003; Mulugeta 1988; Cotton and Koyi 2000). Comparing models A1 and B1, which were shortened orthogonally, our brittle-ductile model B1 is able to better represent the low-angle character of the natural example.

Models of oblique basin inversion show that the use of a ductile layer results in decoupling of the sedimentary cover and a strong localisation of deformation at existing extensional structures (e.g., Del Ventisette et al. 2006; Brun and Nalpas 1996). Similarly, the use of an upper (second) ductile layer (models B2, D2) leads to a decoupling between the upper and lower
480 sediment cover (e.g., Fan et al. 2020; Del Ventisette et al. 2006). As a result, structures within the lower brittle layer are terminated at the upper ductile layer, and do not reach the surface. Consequently, low-angle hinterland-dipping thrusts emerging from the velocity discontinuity are not visible in top view (see e.g., model D2, Figure 11b). Decoupling thus prevents the formation of large-scale structures across the entire sedimentary cover.

5.1.2 Favourable kinematic conditions for basin inversion

485 The movement of the basal plate (i.e., fixed or mobile) greatly influences the structure and location of the resulting wedge in brittle-ductile models (compare e.g., model B1 and B3). By using a mobile plate (model B1), this rigid block acts as a buttress, localizing deformation at the ramp already in the initial stages of the experiment, but also restraining further movement of thrust sheets (Bailey et al. 2002; Héja et al. 2022; Gomes et al. 2010). As a result, further shortening was accommodated along a main back-thrust with multiple fore-thrusts, reflecting the relative movement of the sand layer opposite to the piston. The
490 use of a fixed plate (model B3) represents a thin-skinned deformation style, where the sediment cover and basement are decoupled at a basal décollement. Deformation first localises at the backstop (see also Deng et al. 2020; Yagupsky et al. 2008; Caër 2016), but then propagates to the ramp. The mechanical contrast between the rigid ramp, quartz sand and silicone putty forms a velocity discontinuity (Allemand and Brun 1991; Tron and Brun 1991), which is crucial for localisation during deformation. The step at the ramp, where silicone putty and quartz sand meet, works as a "fault generator" or a "nucleation
495 site for thrust faulting" (Yagupsky et al. 2008, p. 852), not dissimilar to the "thrust mill" of Laubscher (1986), which is also demonstrated in models that use silicone putty or glass microbeads as a weak layer (Caër 2016; Yagupsky et al. 2008). At the same time, structures localizing at the ramp accommodate a large amount of shortening, preventing deformation from propagating further (Caër 2016; Laubscher 1986; Tavarnelli 1996). Therefore, using a thin-skinned deformation style leads to the formation of a low-angle fore-thrust that nucleates at the velocity discontinuity and accommodates a great amount of
500 shortening.

As a prerequisite for fault propagation, the initial wedge at the backstop needs to reach a certain height, analogue to the critical taper theory of Davis et al. (1983). This theory is a popular approach to thrust system mechanics of (foreland) fold-and-thrust belts (Graveleau et al. 2012, and references therein). In all experiments, a wedge of 5.7–7.6 cm high was formed in front of the piston and at least 6 cm of shortening was needed for the thrusts to propagate into the foreland. An alternative approach

505 was provided by Caër (2016), who used a sand prism at the back-stop as pre-existing hinterland topography for brittle-ductile models of basin inversion, resulting in an early propagation of deformation within 0.6 cm of shortening. The early evolution of our analogue models highlights the role of a fold-and-thrust belt in the hinterland for propagation of deformation.

5.1.3 Influence of structural inheritance

Although in all brittle-ductile models with a fixed plate an intial wedge formed parallel to the piston, propagation of

510 deformation led to a series of structures that were oriented parallel to the basal plate boundaries in the subsurface. Models of oblique shortening of pre-existing grabens or steps show similar results, where newly formed reverse and thrust faults more or less outline the structure in the subsurface (e.g., Deng et al. 2020; Yagupsky et al. 2008; Caër 2016). Thrusts in models of Caër (2016) appear to consistently dip towards the backstop. However, PIV analyses of our models show that the dominant strain direction is approximately perpendicular to the thrust trace. The localisation of structures at steps and the geometry of the

515 resulting low-angle fore-thrust with a hanging wall anticline (e.g., model D1, Figure 12a, b) is similar to the models of Caër (2016; their Figure 4.11 b–e) and it is evident that in models with oblique shortening (model D1, D2) thrust faults outline the basal plate structure.

The obliquity angle between the basin axis and subsequent shortening has proven to greatly influence structures formed by basin inversion (Brun and Nalpas 1996; Yagupsky et al. 2008; Del Ventisette et al. 2006; Deng et al. 2020). In purely brittle

520 experiments, low obliquity angles are associated with an increasing angle of the reverse faults (Brun and Nalpas 1996) and dominant fore-thrusts, whereas a higher obliquity angle preferably creates symmetrical pop-up structures (Deng et al. 2020). Our brittle-ductile models were able to create a dominant fore-thrust that localizes at the ramp regardless of the obliquity angle (90° for models B-C, 45° for models D). Fault localisation at subsurface steps was most distinctive in models with a lower obliquity angle (45°, models D). Furthermore, our large-scale models (C and D) agree with those of Yagupsky et al. (2008),

525 where the graben segment closest to the deformation front is reactivated first.

The analogue models prove that low-angle hinterland-dipping thrusts can originate from a pre-existing high-angle normal fault with an opposite dip (see also Figure 5), as predicted (Tavarnelli 1996; Laubscher 1986). A pre-existing network of extensional faults in the subsurface is able to control the geometry of structures related to its inversion. Furthermore, the models exemplify that through localisation of the thrusts at the ramps in the subsurface, the sigmoidal geometry of the Achental thrust hanging

530 wall can be created within a single deformation phase and with a single direction of oblique shortening.

5.2 Comparison with the natural example

In analogue models we aim to create a scaled and simplified version of the natural example, the Achental structure. In the models we show that it is possible to form a sigmoidal structure, characterized by a low-angle main fore-thrust, hanging wall anticlines and a localisation at a pre-existing step, within a single phase of shortening. Model parameters that were found to

535 be applicable to the Achental structure are 1) the presence of a weak basal décollement, 2) thin-skinned deformation, and 3) a clear velocity discontinuity at the frontal ramp acting as a "fault generator". However, laboratory experiments cannot fully encompass the complexities of natural geological structures. In this section, we compare features of the analogue models and the Achental structure.

5.2.1 Mechanical stratigraphy

540 Rheological properties of the sedimentary succession are important parameters for both analogue models and natural processes. A brittle-ductile succession is able to re-create large-scale structures in analogue models. However, small-scale faulting and folding within the sedimentary cover of the NCA is "lost in translation". Comparison between brittle and brittle-ductile models shows that a very weak décollement is imperative for the low-angle Achental thrust to form at a pre-existing basement step. Whether or not this décollement is present in the hanging wall, does not influence localisation of deformation in the models,

545 although it might impact propagation with further shortening (Caër 2016). An offset of the décollement, as opposed to a monocline across the ramp, increases the effect of the velocity discontinuity, but is not strictly necessary for localisation to occur. The Haselgebirge-Reichenhall succession at the base of the Karwendel thrust sheet consisting mostly of rock salt forms the main décollement of the NCA (Eisbacher and Brandner 1995), providing the required weak basal layer. The Kössen Fm may also be represented by a ductile layer, decoupling the lower and upper carbonate platform. However, analogue models

550 show that structures in the lower section do not connect to the upper section. Although in the Achental structure, small-scale folding dies out near the Hauptdolomit-Plattenkalk transition, the overall geometry of the Unnutz anticline is preserved through the entire outcropping sedimentary succession. Therefore, we dismiss the hypothesis that the Kössen Fm behaves as a ductile material.

Because carbonate units of the Achental structure are represented by quartz sand in analogue models, simulating brittle

555 behaviour, the models are not able to simulate folding of the Guffert-Unnutz-Montscheinspitze anticline. Ortner (2003a) proposes a progressive rollover-fault-propagation model (Storti and Salvini 1996) for the Unnutz anticline. This type of folding leads to strongly overturned or recumbent anticlines in fold-and-thrust belts (Storti and Salvini 1996) and involves a fault-propagation fold with strong, layer-parallel shear (flexural slip). Although for fault-propagation folds "important field evidence (…) is the observation that some faults, particularly thrust faults, die out in the cores of folds." (Suppe 1985, p. 350), this is

560 not necessarily the case for progressive rollover-fault-propagation folds, because the overturned limb of the hanging wall anticline has been completely detached from the footwall (Storti and Salvini 1996: Fig. 2). Flexural slip accommodating deformation within the Guffert-Unnutz-Montscheinspitze anticline is seen from layer-parallel and very low-angle fault planes within Hauptdolomit, and support the progressive rollover-fault-propagation model. Fault-propagation folding as a mechanism is seen in the La Roche d'Or anticline, Swiss Alps (Caër 2016). This anticline formed along a thrust fault that, in depth,

565 localises at a basement step attributed to extensional faulting, thus showing strong similarities to the Achental structure. Similar to the Reichenhall-Haselgebirge succession in the NCA, evaporitic sediments form a décollement between the basement and the sediment cover. Martin and Mercier (1996) provide a natural example of the western Jura, showing the development of a low-angle ramp above pre-existing structures of the Bresse graben.

5.2.2 Kinematic parameters and structural inheritance

570 In analogue models, the use of a fixed basal plate translates to a thin-skinned tectonic style, in which the sedimentary cover is decoupled from the basement by a décollement (Rodgers 1949). Such thin-skinned structural style is well known from the NCA (e.g., Eisbacher et al. 1990; Auer and Eisbacher 2003). However, for a correct localisation and propagation of deformation, the presence of a step in the subsurface and topography in the hinterland is important as well. Keeping in mind model scaling, Early Cretaceous topography must have existed at no more than ~ 14 km SE of the Jurassic normal fault. The

575 advancing front of the NCA fold-and-thrust belt and the uplift resulting from movement along the NW-verging Eben thrust (Eisbacher and Brandner 1996) may have provided this topography. Within the subsurface, the Jurassic basin architecture is thought to have provided steps where deformation could localise. Thickness and facies differentiations of Jurassic sediments (Figure 1b) (Schütz 1979; Nagel et al. 1976) underline the presence of such a basin. Following the geometry of the Achental structure, at least one west-dipping normal fault must have been oriented approximately N-S. Strike-slip faults trending E-W

580 (Eisbacher and Brandner 1995, 1996) may form additional steps (Figure 13). Such a basin geometry is similar to Jurassic fault systems in more western parts of the Alpine orogen (Eberli 1987, 1985; Weissert and Bernoulli 1985).

The models were subjected to a single phase of oblique shortening, simulating NW-directed Cretaceous convergence related to Alpine orogeny. Field data from the Achensee area (Sausgruber 1994b; Beer 2003) support the influence of NW-directed shortening. On the other hand, Ortner and Gruber (2011) argue that the offset in the central Achental thrust is larger than in its
585 northern and southern thrust segments, and that the direction of shortening must have been < 270°. Because the orientation of the folds (e.g., the Thiersee syncline; Töchterle 2005) and faults within the Achental structure is oblique to Cretaceous shortening (e.g., Eisbacher and Brandner 1996), many studies have offered alternative hypotheses involving multiple deformation phases and directions (e.g., Spengler 1953; Auer 2001; Ampferer 1921; Fuchs 1944; Channell et al. 1992; Channell et al. 1990; Ortner 2003a). The formation of the Guffert-Unnutz-Montscheinspitze anticline and the Achental thrust
590 is ascribed to pre-Gosau, deformation (Ortner and Gruber 2011; Töchterle 2005), which does not prove that the entire sigmoidal hanging wall formed during a NW direction of shortening. However, in our models we re-create the geometry of the Achental structure by applying shortening at 45° to the N-S trending Jurassic fault, demonstrating that a single uniform phase of oblique shortening is sufficient to create a sigmoidal shape of the hanging wall that outlines the subsurface basin geometry of the Achental structure. Our results thus agree with the hypothesis that the characteristic shape of the Achental structure formed
595 due to forced folding at the borders of a Jurassic basin (Eisbacher and Brandner 1995, 1996; Ortner and Gruber 2011).

One limitation of the analogue models compared to the natural example is that we did not consider Paleogene reactivation of Cretaceous structures. Paleogene folding however, is common throughout the Achental structure and Achensee area. E.g., the Hofjoch, Blaubergalm and Seekar folds (Figure 3) (Eisbacher and Brandner 1995; Brandner and Gruber 2011; Sausgruber 1994b) show an orientation corresponding to post-Cretaceous shortening. The Seekar folds are offset by the N-S striking
600 Seekar fault, which shows dextral strike-slip movement and a P-axis that corresponds to NNE- to NE-directed Paleogene shortening. Paleogene reactivation of fault planes also occurs at the west side of the Achensee (Sausgruber 1994b). Although this post-Cretaceous reactivation may have imprinted on existing structures, we propose that the rough outlines of the Achental structure were established after Cretaceous orogeny (Figure 13).
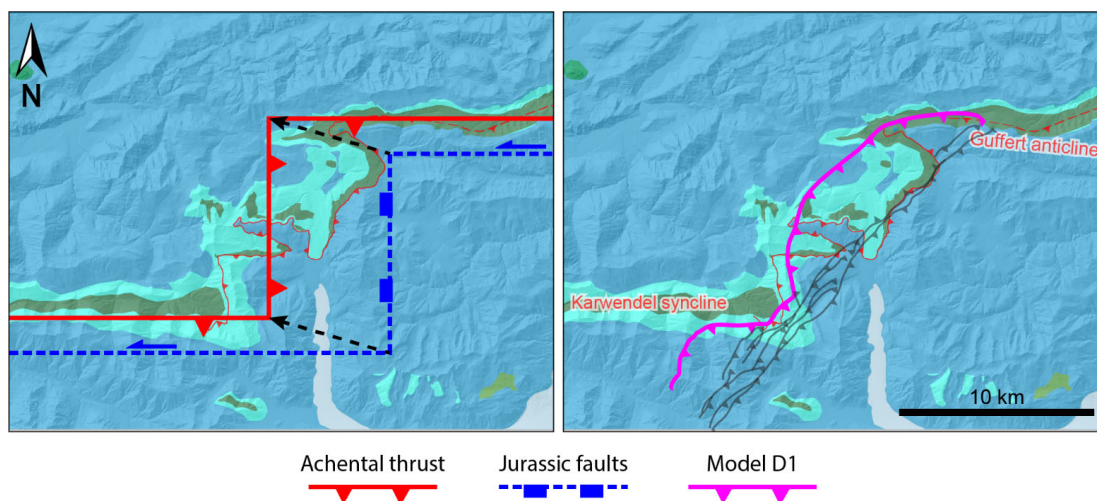
605 **Figure 13:** Summary figure showing possible arrangement of Jurassic basin-bounding faults in relation to the Achental thrust (left) and overlay of inversion structures formed in analogue model D1, outlining the subsurface architecture (right). Modified after Ortner and Gruber (2011) and Ortner and Kilian (2016). For legend of background figure, see Figure 1.

6 Conclusions

Analogue models were used to infer favourable kinematic and mechanic conditions for the oblique inversion of a pre-existing
extensional basin margin. Yet relevant for understanding deformation geometries arising from oblique basin inversion in
general, the modelling results have been discussed in the frame of the Achental structure in the European Alps, which evolved
from the inversion of the Jurassic Achental basin during Alpine orogeny. Based on the modelling results we conclude:

1) A thin-skinned style of deformation that characterises Cretaceous orogeny in the NCA and leads to the formation of a fold-
and-thrust belt in the hinterland, provides the structural framework for propagation of deformation to the basin margins,

2) The Jurassic basin geometry consists of at least (1) an approximately N-S trending, W-dipping normal fault, and (2) two E-
W trending additional strike-slip faults. When applying shortening at 45° to the Jurassic structures, newly formed thrusts then
form along these steps.

3) The sedimentary cover is represented by a brittle succession that is separated from the basement by Aa A ductile
décollement, the (Haselgebirge-Reichenhall succession). This basal décollement is crucial for the decoupling of the
sedimentary cover and is together with the mechanical contrast across the basin bounding normal fault controlling the
localisation of a low-angle thrust dipping opposite to the inherited normal fault, the Achental thrust.

When these parameters are applied, a low-angle thrust, antithetic to the Jurassic normal fault, is formed due to thrust
localisation at the eastern margin of the Achental basin. The hanging wall of this thrust, the Achentaler Schubmasse, outlines
the Jurassic basin architecture in the subsurface, proving that pre-existing extensional faults are a controlling factor for
structures that form during subsequent shortening. Thus, a single phase of oblique shortening at 45° to the Jurassic basin axis
is sufficient to form a sigmoidal geometry of the hanging wall.

Author contributions

The conceptualization of the study was done by HO and EW; Field investigations were performed by WvK, HO, AG and TS;
Analogue modelling was planned and performed by WvK, EW and DS; Data preparation, analysis and visualisation were
performed by WvK; WvK prepared the original draft of the manuscript with input from all co-authors; All co-authors reviewed
and edited the manuscript and approved the final version.

Competing interests

At least one of the (co-)authors is a guest member of the editorial board of Solid Earth and has collaborated as a (co-)author
on publications involving one of the guest editors of Solid Earth. The peer-review process was guided by an independent
editor, and the authors have also no other competing interests to declare.

Acknowledgements

This work was completed as part of a Master Thesis at the University of Innsbruck. The University of Innsbruck through a
needs-based scholarship provided financial support covering fieldwork and travel expenses. Laboratory experiments were
conducted at the TecLab of Utrecht University. We sincerely thank Antoine Auzemery for assistance with the
conceptualization and realization of analogue experiments, as well as fruitful discussions. We also thank Lukas Schifferle for
assistance during fieldwork and digitalization. The authors thank Midland Valley for providing their Move Software in the
frame of their academic software initiative.

Publication bibliography

Allemand, Pascal; Brun, Jean-Pierre (1991): Width of continental rifts and rheological layering of the lithosphere. In
645 *Tectonophysics* 188 (1-2), pp. 63–69. DOI: 10.1016/0040-1951(91)90314-I.

Allen, Janice; Beaumont, Christopher (2016): Continental margin syn-rift salt tectonics at intermediate width margins. In
Basin Res 28 (5), pp. 598–633. DOI: 10.1111/bre.12123.

Amilibia, A.; Mc Clay, Ken; i Montserrat, Francesc Sàbat; Muñoz, J. A.; Roca, Eduard (2005): Analogue modelling of
inverted oblique rift systems. In *Geologica Acta*, p. 251.

650 Ampferer, O. (1902): Über den geologischen Zusammenhang des Karwendel- und Sonnwendgebirges. In *Verhandlungen der
Kaiserlich-Königlichen Geologischen Reichsanstalt*, pp. 104–113.

Ampferer, O. (1912): Gedanken über die Tektonik des Wettersteingebirges. In *Verhandlungen der Kaiserlich-Königlichen
Geologischen Reichsanstalt* 1912, pp. 197–212.

Ampferer, O. (1921): Über NW-Beanspruchungen in den Nordalpen. In *Jahrbuch der Geologischen Bundesanstalt* 71,
655 pp. 198–202.

Ampferer, O. (1941): Tektonische Nachbarschaft Karwendel-Sonnwendgebirge. In *Sitzungsberichte der Akademie der
Wissenschaften in Wien, Mathematisch-Naturwissenschaftliche Klasse* 150, pp. 181–199.

Ampferer, O.; Hammer, W. (1911): Geologischer Querschnitt durch die Alpen vom Allgäu zum Gardasee. In *Jahrbuch der
Kaiserlich-Königlichen Geologischen Reichsanstalt* 61, pp. 531–710.

660 Ampferer, O.; Heissel, G. (1950): Geologische Karte des östlichen Karwendel und des Achensee-Gebietes. Innsbruck:
Universitätsverlag Wagner.

Auer, Matthias (2001): Struktur und Kinematik der nördlichen Kalkalpen im TRANSALP-Profil (Südbayern, Nordtirol).
Dissertation. Universität Karlsruhe, Karlsruhe.

Auer, Matthias; Eisbacher, Gerhard H. (2003): Deep structure and kinematics of the Northern Calcareous Alps (TRANSALP
665 Profile). In *Geol Rundsch* 92 (2), pp. 210–227. DOI: 10.1007/s00531-003-0316-0.

Bachmann, G. H.; Müller, M. (1981): Geologie der Tiefbohrung Vorderriß 1. In *Geologica Bavarica* 81, pp. 17–53.

Bailey, Christopher M.; Giorgis, Scott; Coiner, Lorrie (2002): Tectonic inversion and basement buttressing: an example from
the central Appalachian Blue Ridge province. In *Journal of Structural Geology* 24 (5), pp. 925–936. DOI: 10.1016/S0191-
8141(01)00102-X.

670 Bechstädt, T.; Mostler, H. (1974): Mikrofazies und Mikrofauna mitteltriadischer Beckensedimente der Nördlichen Kalkalpen
Tirols. In *Geologisch-Paläontologische Mitteilungen Universität Innsbruck* 4 (5/6), pp. 1–74.

Beer, E. (2003): Vergleichende tektonische Untersuchungen an zwei längsalpinen Störungen: der Achentaler Schubmasse
und der Salzachstörung. Doctoral thesis. Ludwig-Maximilians-Universität München, Munich, Germany.

Bernoulli, Daniel; Jenkyns, HUGH C. (1974): ALPINE, MEDITERRANEAN, AND CENTRAL ATLANTIC MESOZOIC
675 FACIES IN RELATION TO THE EARLY EVOLUTION OF THE TETHYS. In R. H. Dott, Robert H. Shaver (Eds.):
Modern and Ancient Geosynclinal Sedimentation: SEPM (Society for Sedimentary Geology), pp. 129–160.

Bonini, Marco (1998): Chronology of deformation and analogue modelling of the Plio-Pleistocene 'Tiber Basin':
implications for the evolution of the Northern Apennines (Italy). In *Tectonophysics* 285 (1-2), pp. 147–165. DOI:
10.1016/S0040-1951(97)00189-3.

680   Bonini, Marco; Sani, Federico; Antonielli, Benedetta (2012): Basin inversion and contractional reactivation of inherited normal faults: A review based on previous and new experimental models. In *Tectonophysics* 522-523, pp. 55–88. DOI: 10.1016/j.tecto.2011.11.014.

Bonini, Marco; Sokoutis, Dimitrios; Mulugeta, Genene; Katrivanos, Emmanouil (2000): Modelling hanging wall accommodation above rigid thrust ramps. In *Journal of Structural Geology* 22 (8), pp. 1165–1179. DOI: 10.1016/S0191-
685   8141(00)00033-X.

Brandner, R.; Gruber, A. (2011): Exkursion E2a - Rofangebirge. In A. Gruber (Ed.): Arbeitstagung 2011 "Geologie des Achenseegebietes". Geologisches Kartenblatt 88. Wien: Geologische Bundesanstalt, pp. 149–167.

Brandner, R.; Lotter, M.; Gruber, A.; Ortner, Hugo (2011): Exkursion E3 – Achental – Bächental. Donnerstag, 22.09.2011. In A. Gruber (Ed.): Arbeitstagung 2011 "Geologie des Achenseegebietes". Geologisches Kartenblatt 88. Wien: Geologische
690   Bundesanstalt, pp. 199–224.

Broerse, Taco (2021): Strainmap. Version v1.0.

Broerse, Taco; Krstekanić, Nemanja; Kasbergen, Cor; Willingshofer, Ernst (2021): Mapping and classifying large deformation from digital imagery: application to analogue models of lithosphere deformation. In *Geophysical Journal International* 226 (2), pp. 984–1017. DOI: 10.1093/gji/ggab120.

695   Brun, Jean-Pierre (1999): Narrow rifts versus wide rifts: inferences for the mechanics of rifting from laboratory experiments. In *Philosophical Transactions of the Royal Society of London. Series A: Mathematical, Physical and Engineering Sciences* 357 (1753), pp. 695–712. DOI: 10.1098/rsta.1999.0349.

Brun, Jean-Pierre; Nalpas, Thierry (1996): Graben inversion in nature and experiments. In *Tectonics* 15 (3), pp. 677–687. DOI: 10.1029/95TC03853.

700   Buchanan, P. G.; McClay, K. R. (1992): Experiments on basin inversion above reactivated domino faults. In *Marine and Petroleum Geology* 9 (5), pp. 486–500. DOI: 10.1016/0264-8172(92)90061-I.

Buiter, Susanne J. H.; Pfiffner, Adrian O. (2003): Numerical models of the inversion of half-graben basins. In *Tectonics* 22 (5), n/a-n/a. DOI: 10.1029/2002TC001417.

Caër, T. (2016): Interprétation structurale et équilibre mécanique: Le calcul à la rupture appliqué aux chaînes d'avant-pays.
705   Cas du Jura. Doctoral thesis. Laboratoire Géosciences et Environnement Cergy (GEC, EA 4506), Cergy.

Channell, J. E. T.; Brandner, R.; Spieler, A.; Stoner, J. S. (1992): Paleomagnetism and paleogeography of the northern calcareous Alps (Austria). In *Tectonics* 11 (4), pp. 792–810. DOI: 10.1029/91TC03089.

Channell, J.E.T.; Brandner, R.; Spieler, A. (1990): Mesozoic paleogeography of the Northern Calcareous Alps—Evidence from paleomagnetism and facies analysis. In *Geology* 18 (9), p. 828. DOI: 10.1130/0091-
710   7613(1990)018<0828:MPOTNC>2.3.CO;2.

Cooper, Mark; Warren, Marian J. (2020): Inverted fault systems and inversion tectonic settings. In Nicola Scarselli, J. Adam, Domenico Chiarella, David G. Roberts, Albert W. Bally (Eds.): Regional Geology and Tectonics: Principles of Geologic Analysis: Elsevier, pp. 169–204.

Cotton, J. T.; Koyi, H. A. (2000): Modeling of thrust fronts above ductile and frictional detachments: Application to
715   structures in the Salt Range and Potwar Plateau, Pakistan. In *Geological Society of America Bulletin* 112 (3), pp. 351–363. DOI: 10.1130/0016-7606(2000)112<351:MOTFAD>2.0.CO;2.

Czurda, K.; Nicklas, N. (1971): Zur Mikrofazies und Mikrostratigraphie des Hauptdolomits und Plattenkalk-Niveaus der Klostertaler Alpen und des Rhätikon (Nördliche Kalkalpen, Vorarlberg). In H. Mostler (Ed.): Beiträge zur Mikrofazies und Stratigraphie von Tirol und Vorarlberg. Festband des Geol. Inst., 300-Jahr- Feier Univ. Innsbruck. Innsbruck, pp. 165–253.

720 Davis, Dan; Suppe, John; Dahlen, F. A. (1983): Mechanics of fold-and-thrust belts and accretionary wedges. In *J. Geophys. Res.* 88 (B2), p. 1153. DOI: 10.1029/JB088iB02p01153.

Del Ventisette, Chiara; Montanari, Domenico; Sani, Federico; Bonini, Marco (2006): Basin inversion and fault reactivation in laboratory experiments. In *Journal of Structural Geology* 28 (11), pp. 2067–2083. DOI: 10.1016/J.JSG.2006.07.012.

Del Ventisette, Chiara; Montanari, Domenico; Sani, Federico; Bonini, Marco; Corti, Giacomo (2007): Reply to comment by
725 J. Wickham on "Basin inversion and fault reactivation in laboratory experiments". In *Journal of Structural Geology* 29 (8), pp. 1417–1418. DOI: 10.1016/j.jsg.2007.05.003.

Deng, Hongling; Koyi, Hemin A.; Zhang, Jinjiang (2020): Modelling oblique inversion of pre-existing grabens. In *Geological Society, London, Special Publications* 487 (1), pp. 263–290. DOI: 10.1144/SP487.5.

Dombrádi, Endre; Sokoutis, Dimitrios; Bada, Gábor; Cloetingh, Sierd; Horváth, Frank (2010): Modelling recent deformation
730 of the Pannonian lithosphere: Lithospheric folding and tectonic topography. In *Tectonophysics* 484 (1-4), pp. 103–118. DOI: 10.1016/j.tecto.2009.09.014.

Donofrio, D. A.; Brandner, R.; Poleschinski, W. (2003): Conodonten der Seefeld-Formation: ein Beitrag zur Bio- und Lithostratigraphie der Hauptdolomit-Plattform (Obertrias, westliche Nördliche Kalkalpen, Tirol. In *Geologisch-Paläontologische Mitteilungen Universität Innsbruck* 26, pp. 91–107.

735 Dubois, Agnès; Odonne, Francis; Massonnat, Gérard; Lebourg, Thomas; Fabre, Richard (2002): Analogue modelling of fault reactivation: tectonic inversion and oblique remobilisation of grabens. In *Journal of Structural Geology* 24 (11), pp. 1741–1752. DOI: 10.1016/S0191-8141(01)00129-8.

Eberli, Gregor Paul (1985): Die jurassischen Sedimente in den ostalpinen Decken Graubündens: Relikte eines passiven Kontinentalrandes. ETH Zurich.

740 Eberli, Gregor Paul (1987): Carbonate turbidite sequences deposited in rift-basins of the Jurassic Tethys Ocean (eastern Alps, Switzerland). In *Sedimentology* 34 (3), pp. 363–388. DOI: 10.1111/j.1365-3091.1987.tb00576.x.

Eberli, Gregor Paul; Bernoulli, Daniel; Sanders, D.; Vecsei, A. (1993): From aggradation to progradation: The Maiella platform, Abruzzi, Italy. In T. Simo, R. W. Scott (Eds.): Cretaceous Carbonate Platforms (AAPG Memoir, 56).

Eisbacher, Gerhard H.; Brandner, R. (1995): Role of high-angle faults during heteroaxial contraction, Inntal thrust sheet,
745 Northern Calcareous Alps, western Austria. In *Geologisch-Paläontologische Mitteilungen Universität Innsbruck* 20, pp. 389–406.

Eisbacher, Gerhard H.; Brandner, R. (1996): Superposed fold-thrust structures and high-angle faults, Northwestern Calcareous Alps, Austria. In *Eclogae geol. Helv.* 89, pp. 553–571.

Eisbacher, Gerhard H.; Linzer, Hans-Gert; Meier, L. (1990): A depth extrapolated structural transect across the Northern
750 Calcareous Alps of Western Tirol. In *Eclogae geol. Helv.* 83 (3), pp. 711–725.

Etheridge, M. A. (1986): On the reactivation of extensional fault systems. In *Phil. Trans. R. Soc. Lond. A* 317 (1539), pp. 179–194. DOI: 10.1098/rsta.1986.0031.

Fan, Xiaogen; Jia, Dong; Yin, Hongwei; Shen, Li; Liu, Jun; Cui, Jian et al. (2020): Analogue modeling of the northern Longmen Shan thrust belt (eastern margin of the Tibetan plateau) and strain analysis based on Particle Image Velocimetry. In *Journal of Asian Earth Sciences* 198, p. 104238. DOI: 10.1016/j.jseaes.2020.104238.

Faupl, P.; Wagreich, M. (1999): Late Jurassic to Eocene Palaeogeography and Geodynamic Evolution of the Eastern Alps. In *Mitteilungen der Österreichischen Geologischen Gesellschaft* 92, pp. 79–94.

Flügel, Erik (2010): Microfacies of Carbonate Rocks. Berlin, Heidelberg: Springer Berlin Heidelberg.

Froitzheim, Nikolaus; Manatschal, Gianreto (1996): Kinematics of Jurassic rifting, mantle exhumation, and passive-margin formation in the Austroalpine and Penninic nappes (eastern Switzerland). In *Geological Society of America Bulletin* 108 (9), pp. 1120–1133. DOI: 10.1130/0016-7606(1996)108<1120:KOJRME>2.3.CO;2.

Froitzheim, Nikolaus; Schmid, Stefan M.; Conti, Paolo (1994): Repeated change from crustal shortening to orogen-parallel extension in the Austroalpine units of Graubünden. DOI: 10.5169/seals-167471.

Fruth, I.; Scherreiks, R. (1982): Hauptdolomit (Norian) — stratigraphy, paleogeography and diagenesis. In *Sedimentary Geology* 32 (3), pp. 195–231. DOI: 10.1016/0037-0738(82)90050-1.

Fuchs, A. (1944): Untersuchungen am tektonischen Gefüge der Tiroler Alpen. II. (Kalkalpen Achensee – Kaisergebirge). In *Neues Jahrb. für Mineral. etc. Abh., Abt. B* 88, pp. 337–373.

Gawlick, H.-J. (2004): Definition of the Tauglboden Formation (Oxfordian to Tithonian) in the Tauglboden Basin (Northern Calcareous Alps). In *Berichte des Institutes für Erdwissenschaften der Karl-Franzens-Universität Graz* 9 (127-129).

Golebiowski, R. (1991): Becken und Riffe der alpinen Obertrias. Lithostratigraphie und Biofazies der Kössener Formation. Exkursionen im Jungpaläozoikum und Mesozoikum Österreichs. Wien: Österreichische Paläontologische Gesellschaft.

Gomes, Caroline J.S.; Danderfer Filho, André; Posada, Ana Maria A.; Da Silva, Anielle C. (2010): The role of backstop shape during inversion tectonics physical models. In *An. Acad. Bras. Ciênc.* 82 (4), pp. 997–1012. DOI: 10.1590/S0001-37652010000400021.

Granado, Pablo; Roca, Eduard; Strauss, Philipp; Pelz, Klaus; Muñoz, Josep Anton (2019): Structural styles in fold-and-thrust belts involving early salt structures: The Northern Calcareous Alps (Austria). In *Geology* 47 (1), pp. 51–54. DOI: 10.1130/G45281.1.

Graveleau, Fabien; Malavieille, Jacques; Dominguez, Stéphane (2012): Experimental modelling of orogenic wedges: A review. In *Tectonophysics* 538-540, pp. 1–66. DOI: 10.1016/j.tecto.2012.01.027.

Gruber, A. (2011): Geological manuscript map ÖK 88 Achenkirch. Unveröff. Manuskriptkarte. Wien: Geologische Bundesanstalt.

Gruber, Alfred; Lotter, Michael; Geologische Bundesanstalt (2022): Erläuterungen zu Blatt 88 Achenkirch. Wien: Geologische Bundesanstalt (Geologische Karte der Republik Österreich [Geologische Karte Österreich / Erläuterungen] : Erläuterungen).

Gümbel, C. W. (1861): Geognostische Beschreibung des bayerischen Alpengebirges und seines Vorlandes. Gotha: Perthes.

Haas, J.; Kovács, S.; Krystyn, L.; Lein, R. (1995): Significance of Late Permian-Triassic facies zones in terrane reconstructions in the Alpine-North Pannonian domain. In *Tectonophysics* 242 (1-2), pp. 19–40. DOI: 10.1016/0040-1951(94)00157-5.

Hahn, F. Felix (1912): Versuch einer Gliederung der austroalpinen Masse westlich der österreichischen Traun. In *Verhandlungen der Kaiserlich-Königlichen Geologischen Reichsanstalt* 1912, pp. 337–344.

Hahn, F. Felix (1913a): Grundzüge des Baues der nördlichen Kalkalpen zwischen Inn und Enns, I. Teil. In *Mitteilungen der Österreichischen Geologischen Gesellschaft* 9, pp. 238–357.

Hahn, F. Felix (1913b): Grundzüge des Baues der nördlichen Kalkalpen zwischen Inn und Enns, II. Teil. In *Mitteilungen der Österreichischen Geologischen Gesellschaft* 9, pp. 374–500.

Heißel, W. (1958): Zur Tektonik der Nordtiroler Kalkalpen. In *Mitteilungen der Österreichischen Geologischen Gesellschaft* 50 (1957), pp. 95–132.

Héja, G.; Ortner, H.; Fodor, L.; Németh, A.; Kövér, S. (2022): Modes of Oblique Inversion: A Case Study From the Cretaceous Fold and Thrust Belt of the Western Transdanubian Range (TR), West Hungary. In *Tectonics* 41 (3). DOI: 10.1029/2021TC006728.

Hornung, T.; Brandner, R.; Krystyn, L.; Joachimski, M.; Keim, L. (2007): Multistratigraphic constraints on the NW Tethyan "Carnian Crisis". In S. G. Lucas, J. A. Spielmann (Eds.): The Global Triassic. Albuquerque: New Mexico Museum of Natural History, pp. 59–67.

Hubbert, M. K. (1937): Theory of scale models as applied to the study of geologic structures. In *Geological Society of America Bulletin* 48 (10), pp. 1459–1520. DOI: 10.1130/GSAB-48-1459.

Jerz, H. (1966): Untersuchungen über Stoffbestand, Bildungsbedingungen und Paläogeographie der Raibler Schichten zwischen Lech und Inn (Nördl. Kalkalpen). In *Geologica Bavarica* 56, pp. 3–100.

Kilian, Sinah (2013): Bericht 2012 über geologische und strukturgeologische Aufnahmen im Karwendelgebirge auf Blatt 2223 Innsbruck und auf Blatt 2217 Hinterriß. In *Jahrbuch der Geologischen Bundesanstalt* 153, pp. 411–417.

Kilian, Sinah; Ortner, Hugo (2019): Structural evidence of in-sequence and out-of-sequence thrusting in the Karwendel mountains and the tectonic subdivision of the western Northern Calcareous Alps. In *Austrian Journal of Earth Sciences* 112 (1), pp. 62–83. DOI: 10.17738/ajes.2019.0005.

Kilian, Sinah; Ortner, Hugo; Schneider-Muntau, Barbara (2021): Buckle folding in the Northern Calcareous Alps - Field observations and numeric experiments. In *Journal of Structural Geology* 150, p. 104416. DOI: 10.1016/j.jsg.2021.104416.

Kley, Jonas; Rossello, Eduardo A.; Monaldi, César R.; Habighorst, Björn (2005): Seismic and field evidence for selective inversion of Cretaceous normal faults, Salta rift, northwest Argentina. In *Tectonophysics* 399 (1-4), pp. 155–172. DOI: 10.1016/J.TECTO.2004.12.020.

Konstantinovskaya, Elena A.; Harris, Lyal B.; Poulin, Jimmy; Ivanov, Gennady M. (2007): Transfer zones and fault reactivation in inverted rift basins: Insights from physical modelling. In *Tectonophysics* 441 (1-4), pp. 1–26. DOI: 10.1016/j.tecto.2007.06.002.

Koopman, A.; Speksnijder, A.; Horsfield, W. T. (1987): Sandbox model studies of inversion tectonics. In *Tectonophysics* 137 (1-4), pp. 379–388. DOI: 10.1016/0040-1951(87)90329-5.

Krainer, K.; Lucas, S. G.; Strasser, M. (2011): Vertebrate Fossils from the Northalpine Raibl Beds, Western Northern Calcareous Alps, Tyrol (Austria). In *Austrian Journal of Earth Sciences* 104 (1), pp. 97–106.

Krstekanić, Nemanja; Willingshofer, Ernst; Broerse, Taco; Matenco, Liviu; Toljić, Marinko; Stojadinovic, Uros (2021): Analogue modelling of strain partitioning along a curved strike-slip fault system during backarc-convex orocline formation:

Implications for the Cerna-Timok fault system of the Carpatho-Balkanides. In *Journal of Structural Geology* 149, p. 104386. DOI: 10.1016/j.jsg.2021.104386.

Krstekanić, Nemanja; Willingshofer, Ernst; Matenco, Liviu; Toljić, Marinko; Stojadinovic, Uros (2022): The influence of back-arc extension direction on the strain partitioning associated with continental indentation: Analogue modelling and 830 implications for the Circum-Moesian Fault System of South-Eastern Europe. In *Journal of Structural Geology* 159, p. 104599. DOI: 10.1016/j.jsg.2022.104599.

Lackschewitz, Klas S.; Grützmacher, Uwe; Henrich, Rüdiger (1991): Paleoceanography and rotational block faulting in the Jurassic carbonate series of the Chiemgau Alps (Bavaria). In *Facies* 24 (1), pp. 1–23. DOI: 10.1007/BF02536838.

Laubscher, H. P. (1986): The eastern Jura: Relations between thin-skinned and basement tectonics, local and regional. In 835 *Geol Rundsch* 75 (3), pp. 535–553. DOI: 10.1007/BF01820630.

Lee, A. R.; Warren, J. B. (1940): A coni-cylindrical viscometer for measuring the visco-elastic characteristics of highly viscous liquids. In *J. Sci. Instrum.* 17 (3), pp. 63–67. DOI: 10.1088/0950-7671/17/3/303.

Leever, Karen A.; Gabrielsen, Roy H.; Faleide, Jan Inge; Braathen, Alvar (2011): A transpressional origin for the West Spitsbergen fold-and-thrust belt: Insight from analog modeling. In *Tectonics* 30 (2), n/a-n/a. DOI: 10.1029/2010TC002753.

840 Lein, R. (1987): Evolution of the Northern Calcareous Alps during Triassic times. In H. W. Flügel, P. Faupl (Eds.): Geodynamics of the Eastern Alps. Wien: Deuticke, pp. 85–102.

Leitner, C.; Neubauer, F. (2011): Tectonic significance of structures within the salt deposits Altaussee and Berchtesgaden– Bad Dürrnberg, Northern Calcareous Alps. In *Austrian Journal of Earth Sciences* 104 (2), pp. 2–21.

Lemoine, Marcel; Bas, Thierry; Arnaud-Vanneau, Annie; Arnaud, Hubert; Dumont, Thierry; Gidon, Maurice et al. (1986): 845 The continental margin of the Mesozoic Tethys in the Western Alps. In *Marine and Petroleum Geology* 3 (3), pp. 179–199. DOI: 10.1016/0264-8172(86)90044-9.

Lipold, M. W. (1854): Der Salzberg am Dürrnberg nächst Hallein. In *Jahrbuch der Kaiserlich-Königlichen Geologischen Reichsanstalt* 5, pp. 590–610.

Lotter, M.; Gruber, A. (2011): Gravitate Massenbewegungen in der Karwendel- und in der Thiersee Synklinale auf ÖK 88 850 Achenkirch mit Schwerpunkt Einzugsgebiet des Kesselbaches (Bächental). In A. Gruber (Ed.): Arbeitstagung 2011 "Geologie des Achenseegebietes". Geologisches Kartenblatt 88. Wien: Geologische Bundesanstalt, pp. 89–107.

Manger, G. E. (1963): Porosity and bulk density of sedimentary rocks. Edited by United States Geological Survey (USGS) (Geological Survey Bulletin, 1144-E).

Martin, Jacques; Mercier, Eric (1996): Heritage distensif et structuration chevauchante dans une chaine de couverture; apport 855 de l'equilibrage par modelisation geometrique dans le Jura nord-occidental. In *Bulletin de la Société Géologique de France* 167 (1), pp. 101–110.

Merle, Olivier; Abidi, Nadia (1995): Approche experimentale du fonctionnement des rampes emergentes. In *Bulletin de la Société Géologique de France* 166 (5), pp. 439–450. DOI: 10.2113/gssgfbull.166.5.439.

Mojsisovics, E. von (1871): Beiträge zur topischen Geologie der Alpen. In *Jahrbuch der Geologischen Reichsanstalt* 21, 860 pp. 189–210.

Mooney, M.; Ewart, R. H. (1934): The Conicylindrical Viscometer. In *Physics* 5 (11), pp. 350–354. DOI: 10.1063/1.1745219.

Müller-Jungbluth, W.-U. (1968): Sedimentary Petrologic Investigation of the Upper Triassic "Hauptdolomit" of the Lechtaler Alps, Tyrol, Austria. In G. Müller, G. M. Friedman (Eds.): Recent Developments in Carbonate Sedimentology in Central Europe. Berlin, Heidelberg: Springer Berlin Heidelberg, pp. 228–239.

Mulugeta, Genene (1988): Modelling the geometry of Coulomb thrust wedges. In *Journal of Structural Geology* 10 (8), pp. 847–859. DOI: 10.1016/0191-8141(88)90099-5.

Nagel, K.-H. (1975): Der Bau der Thiersee- und Karwendelmulde (Tirol). Stuttgart (Geotektonische Forschungen, 48).

Nagel, K.-H.; Schütz, K.-I.; Schütz, S.; Wilmers, W.; Zeil, W. (1976): Die geodynamische Entwicklung der Thiersee- und der Karwendelmulde (Nördliche Kalkalpen). In *Geol Rundsch* 65, pp. 536–557.

Nielsen, Søren B.; Hansen, David L. (2000): Physical explanation of the formation and evolution of inversion zones and marginal troughs. In *Geology* 28 (10), p. 875. DOI: 10.1130/0091-7613(2000)28<875:PEOTFA>2.0.CO;2.

Nittel, P. (2006): Beiträge zur Stratigraphie und Mikropaläontologie der Mitteltrias der Innsbrucker Nordkette (Nördliche Kalkalpen, Austria). In *Geo.Alp* 3, pp. 93–145.

Ortner, Hugo (2001): Growing folds and sedimentation of the Gosau Group, Muttekopf, Northern Calcareous Alps, Austria. In *Geol Rundsch* 90 (3), pp. 727–739. DOI: 10.1007/s005310000182.

Ortner, Hugo (2003a): Cretaceous thrusting in the western part of the Northern Calcareous Alps (Austria) - evidences from synorogenic sedimentation and structural data. In *Mitteilungen der Österreichischen Geologischen Gesellschaft* 94 (2001), pp. 63–77.

Ortner, Hugo (2003b): Local and far field stress-analysis of brittle deformation in the western part of the Northern Calcareous Alps, Austria. In *Geologisch-Paläontologische Mitteilungen Universität Innsbruck* 26, pp. 109–136.

Ortner, Hugo (2016): Field trip 4 Deep water sedimentation on top of a growing orogenic wedge - interaction of thrusting, erosion and deposition in the Cretaceous Northern Calcareous Alps. In *Geo.Alp* 13, pp. 141–182.

Ortner, Hugo; Gaupp, R. (2007): Synorogenic sediments of the western Northern Calcareous Alps. In *Geo.Alp* 4, pp. 133–148.

Ortner, Hugo; Gruber, A. (2011): 3D-Geometrie der Strukturen zwischen Karwendel-Synklinale und Thiersee-Synklinale. In A. Gruber (Ed.): Arbeitstagung 2011 "Geologie des Achenseegebietes". Geologisches Kartenblatt 88. Wien: Geologische Bundesanstalt, pp. 51–67.

Ortner, Hugo; Kilian, Sinah (2016): Sediment creep on slopes in pelagic limestones: Upper Jurassic of Northern Calcareous Alps, Austria. In *Sedimentary Geology* 344, pp. 350–363. DOI: 10.1016/J.SEDGEO.2016.03.013.

Ortner, Hugo; Kilian, Sinah (2022): Thrust tectonics in the Wetterstein and Mieming mountains, and a new tectonic subdivision of the Northern Calcareous Alps of Western Austria and Southern Germany. In *Geol Rundsch* 111 (2), pp. 543–571. DOI: 10.1007/s00531-021-02128-3.

Ortner, Hugo; Kositz, Andreas; Willingshofer, Ernst; Sokoutis, Dimitrios (2016): Geometry of growth strata in a transpressive fold belt in field and analogue model: Gosau Group at Muttekopf, Northern Calcareous Alps, Austria. In *Basin Res* 28 (6), pp. 731–751. DOI: 10.1111/bre.12129.

Ortner, Hugo; Sieberer, Anna-Katharina (2022): From foreland thrust belt to accretionary wedge: Synorogenic sediments monitor a changing geodynamic setting in the Northern Calcareous Alps of the European Eastern Alps.

Ortner, Hugo; Ustaszewski, Michaela; Rittner, Martin (2008): Late Jurassic tectonics and sedimentation: breccias in the
900 Unken syncline, central Northern Calcareous Alps. In *Swiss J. Geosci.* 101 (S1), pp. 55–71. DOI: 10.1007/s00015-008-1282-
0.

Persson, Katarina S.; Sokoutis, Dimitrios (2002): Analogue models of orogenic wedges controlled by erosion. In
Tectonophysics 356 (4), pp. 323–336. DOI: 10.1016/S0040-1951(02)00443-2.

Piller, W. E.; Egger, H.; Erhart, C. W.; Gross, M.; Harzhauser, M.; Hubmann, B. et al. (2004): Die stratigraphische Tabelle
905 von Österreich 2004 (sedimentäre Schichtfolgen). Wien: Kommission für die paläontologische und stratigraphische
Erforschung Österreichs der Österreichischen Akademie der Wissenschaften und Österreichische Stratigraphische
Kommission.

Quenstedt, W. (1933): Studien in der Überschiebungszone von Achenkirch. In *Zeitschrift der Deutschen Geologischen
Gesellschaft* 85, pp. 459–461.

910 Ramberg, Hans (1981): Gravity, deformation and the earth's crust. In theory, experiments and geological application. 2nd ed.
London: Academic Press.

Riedel, Peter (1988): Facies and development of the 'wilde kirche' reef complex (Rhaetian, Upper Triassic,
Karwendelgebirge, Austria). In *Facies* 18 (1), pp. 205–217. DOI: 10.1007/BF02536800.

Rodgers, John (1949): Evolution of Thought on Structure of Middle and Southern Appalachians. In *Bulletin* 33. DOI:
915 10.1306/3D933E00-16B1-11D7-8645000102C1865D.

Rüffer, T.; Zühlke, R. (1995): Sequence Stratigraphy and Sea-Level Changes in the Early to Middle Triassic of the Alps: A
Global Comparison. In B.U Haq (Ed.): Sequence Stratigraphy and Depositional Response to Eustatic, Tectonic and Climatic
Forcing. Dordrecht: Kluwer, pp. 161–207.

Sassi, W.; Colletta, B.; Balé, P.; Paquereau, T. (1993): Modelling of structural complexity in sedimentary basins: The role of
920 pre-existing faults in thrust tectonics. In *Tectonophysics* 226 (1-4), pp. 97–112. DOI: 10.1016/0040-1951(93)90113-X.

Sausgruber, T. (1994a): Bericht 1993 über geologische Aufnahmen in den Nördlichen Kalkalpen auf Blatt 88 Achenkirch. In
Jahrbuch der Geologischen Bundesanstalt 137, p. 469.

Sausgruber, T. (1994b): Jurabeckenentwicklung nördlich vom Achensee und deren Folgen bei der alpidischen
Kompressionstektonik. Diploma thesis. Leopold-Franzens Universität Innsbruck, Innsbruck.

925 Schmid, Stefan M.; Bernoulli, Daniel; Fügenschuh, Bernhard; Matenco, Liviu; Schefer, Senecio; Schuster, Ralf et al. (2008):
The Alpine-Carpathian-Dinaridic orogenic system: correlation and evolution of tectonic units. In *Swiss J. Geosci.* 101 (1),
pp. 139–183. DOI: 10.1007/s00015-008-1247-3.

Schmid, Stefan M.; Fügenschuh, Bernhard; Kissling, Eduard; Schuster, Ralf (2004): Tectonic map and overall architecture
of the Alpine orogen. In *Eclogae geol. Helv.* 97 (1), pp. 93–117. DOI: 10.1007/s00015-004-1113-x.

930 Schmid, Stefan M.; Pfiffner, O. A.; Froitzheim, Nikolaus; Schönborn, G.; Kissling, Eduard (1996): Geophysical-geological
transect and tectonic evolution of the Swiss-Italian Alps. In *Tectonics* 15 (5), pp. 1036–1064. DOI: 10.1029/96TC00433.

Schütz, K.-I. (1979): Die Aptychenschichten der Thiersee- und der Karwendel-Mulde. In *Geotektonische Forschungen* 57,
pp. 1–84.

Sibson, Richard H. (1995): Selective fault reactivation during basin inversion: potential for fluid redistribution through fault-
935 valve action. In *Geological Society, London, Special Publications* 88 (1), pp. 3–19. DOI: 10.1144/GSL.SP.1995.088.01.02.

Smit, J. H. W. (2005): Brittle-ductile coupling in thrust wedges and continental transforms. Doctoral thesis. VU Amsterdam & Université de Rennes, Amsterdam, Rennes.

Smit, J. H. W.; Brun, Jean-Pierre; Sokoutis, Dimitrios (2003): Deformation of brittle-ductile thrust wedges in experiments and nature. In *J. Geophys. Res.* 108 (B10). DOI: 10.1029/2002JB002190.

940   Sokoutis, Dimitrios; Bonini, Marco; Medvedev, Sergei; Boccaletti, Mario; Talbot, Christopher J.; Koyi, Hemin (2000): Indentation of a continent with a built-in thickness change: experiment and nature. In *Tectonophysics* 320 (3-4), pp. 243–270. DOI: 10.1016/S0040-1951(00)00043-3.

Sokoutis, Dimitrios; Burg, Jean-Pierre; Bonini, Marco; Corti, Giacomo; Cloetingh, Sierd (2005): Lithospheric-scale structures from the perspective of analogue continental collision. In *Tectonophysics* 406 (1-2), pp. 1–15. DOI:
945   10.1016/J.TECTO.2005.05.025.

Spengler, E. (1953): Versuch einer Rekonstruktion des Ablagerungsraumes der nördlichen Kalkalpen (1. Teil, Westabschnitt). In *Jahrbuch der Geologischen Bundesanstalt* 96, pp. 1–64.

Spengler, E. (1956): Versuch einer Rekonstruktion des Ablagerungsraumes der nördlichen Kalkalpen (2. Teil, Mittelabschnitt). In *Jahrbuch der Geologischen Bundesanstalt* 99, pp. 1–74.

950   Spieler, A. (1994): Bericht 1993 über geologische Aufnahmen in den Nördlichen Kalkalpen auf Blatt 88 Achenkirch. In *Jahrbuch der Geologischen Bundesanstalt* 137, pp. 474–475.

Spieler, A. (1995): Geological manuscript map.

Spieler, A.; Brandner, R. (1989): Vom Jurassischen Pull-apart Becken zur Westüberschiebung der Achentaler Schubmasse (Tirol, Österreich). In *Geologisch-Paläontologische Mitteilungen Universität Innsbruck* 16, pp. 191–194.

955   Spötl, Christoph (1989): The Alpine Haselgebirge Formation, Northern Calcareous Alps (Austria): Permo-Scythian evaporites in an alpine thrust system. In *Sedimentary Geology* 65 (1-2), pp. 113–125. DOI: 10.1016/0037-0738(89)90009-2.

Stampfli, G.M; Mosar, J.; Marquer, D.; Marchant, R.; Baudin, T.; Borel, G. (1998): Subduction and obduction processes in the Swiss Alps. In *Tectonophysics* 296 (1-2), pp. 159–204. DOI: 10.1016/S0040-1951(98)00142-5.

Storti, Fabrizio; Salvini, Francesco (1996): Progressive Rollover Fault-Propagation Folding: A Possible Kinematic
960   Mechanism to Generate Regional-Scale Recumbent Folds in Shallow Foreland Belts. In *Bulletin* 80. DOI: 10.1306/64ED8782-1724-11D7-8645000102C1865D.

Stüwe, Kurt; Schuster, Ralf (2010): Initiation of subduction in the Alps: Continent or ocean? In *Geology* 38 (2), pp. 175–178. DOI: 10.1130/G30528.1.

Suppe, John (1985): Principles of structural geology. Englewood Cliffs, New Jersey: Prentice-Hall.

965   Tavarnelli, E. (1996): The effects of pre-existing normal faults on thrust ramp development: An example from the northern Apennines, Italy. In *Geol Rundsch* 85 (2), pp. 363–371. DOI: 10.1007/BF02422241.

Thielicke, William (2014): The Flapping Flight of Birds - Analysis and Application. Phd thesis. Rijksuniversiteit Groningen, Groningen, Netherlands. Available online at http://irs.ub.rug.nl/ppn/382783069.

Thielicke, William; Sonntag, René (2021): Particle Image Velocimetry for MATLAB: Accuracy and enhanced algorithms in
970   PIVlab. In *JORS* 9 (1), p. 12. DOI: 10.5334/jors.334.

Thielicke, William; Stamhuis, Eize J. (2014): PIVlab – Towards User-friendly, Affordable and Accurate Digital Particle Image Velocimetry in MATLAB. In *Journal of Open Research Software* 2. DOI: 10.5334/jors.bl.

Thorwart, Martin; Dannowski, Anke; Grevemeyer, Ingo; Lange, Dietrich; Kopp, Heidrun; Petersen, Florian et al. (2021): Basin inversion: reactivated rift structures in the central Ligurian Sea revealed using ocean bottom seismometers. In *Solid Earth* 12 (11), pp. 2553–2571. DOI: 10.5194/se-12-2553-2021.

Töchterle, A. (2005): Tektonische Entwicklungsgeschichte des Südteiles der Nördlichen Kalkalpen entlang der TRANSALP-Tiefenseismik anhand bilanzierter Profile. Diploma thesis. Leopold-Franzens Universität Innsbruck, Innsbruck.

Tollmann, A. (1970): Tektonische Karte der Nördlichen Kalkalpen, 3. Teil: Der Westabschnitt. In *Mitteilungen der Österreichischen Geologischen Gesellschaft* 62 (1969), pp. 78–170.

Tollmann, A. (1973): Monographie der Nördlichen Kalkalpen. Grundprinzipien der alpinen Deckentektonik. Eine Systemanalyse am Beispiel der Nördlichen Kalkalpen. Wien: Deuticke.

Tollmann, A. (1976): Der Bau der Nördlichen Kalkalpen. Monographie der Nördlichen Kalkalpen, Teil III. Wien: Deuticke.

Tong, Hengmao; an Yin (2011): Reactivation tendency analysis: A theory for predicting the temporal evolution of preexisting weakness under uniform stress state. In *Tectonophysics* 503 (3-4), pp. 195–200. DOI: 10.1016/j.tecto.2011.02.012.

Tron, Virginie; Brun, Jean-Pierre (1991): Experiments on oblique rifting in brittle-ductile systems. In *Tectonophysics* 188 (1-2), pp. 71–84. DOI: 10.1016/0040-1951(91)90315-J.

Turner, J. P.; Williams, G. A. (2004): Sedimentary basin inversion and intra-plate shortening. In *Earth-Sci. Rev.* 65, pp. 277–304.

Ulrich, R. (1960): Die Entwicklung der ostalpinen Juraformation im Vorkarwendel zwischen Mittenwald und Achensee. In *Geologica Bavarica* 41, pp. 99–151.

van Gelder, I. E.; Willingshofer, E.; Sokoutis, D.; Cloetingh, S.A.P.L. (2017): The interplay between subduction and lateral extrusion: A case study for the European Eastern Alps based on analogue models. In *Earth and Planetary Science Letters* 472, pp. 82–94. DOI: 10.1016/j.epsl.2017.05.012.

Weijermars, R. (1986a): Finite strain of laminar flows can be visualized in SGM36-polymer. In *Naturwissenschaften* 73 (1), pp. 33–34. DOI: 10.1007/BF01168803.

Weijermars, R.; Jackson, M.P.A.; Vendeville, B. (1993): Rheological and tectonic modeling of salt provinces. In *Tectonophysics* 217 (1-2), pp. 143–174. DOI: 10.1016/0040-1951(93)90208-2.

Weijermars, Ruud (1986b): Flow behaviour and physical chemistry of bouncing putties and related polymers in view of tectonic laboratory applications. In *Tectonophysics* 124 (3-4), pp. 325–358. DOI: 10.1016/0040-1951(86)90208-8.

Weijermars, Ruud (1986c): Polydimethylsiloxane flow defined for experiments in fluid dynamics. In *Appl. Phys. Lett.* 48 (2), pp. 109–111. DOI: 10.1063/1.97008.

Weijermars, Ruud; Schmeling, Harro (1986): Scaling of Newtonian and non-Newtonian fluid dynamics without inertia for quantitative modelling of rock flow due to gravity (including the concept of rheological similarity). In *Physics of the Earth and Planetary Interiors* 43 (4), pp. 316–330. DOI: 10.1016/0031-9201(86)90021-X.

Weissert, Helmut J.; Bernoulli, Daniel (1985): A transform margin in the Mesozoic Tethys: evidence from the Swiss Alps. In *Geol Rundsch* 74 (3), pp. 665–679. DOI: 10.1007/BF01821220.

Wickham, John (2007): Comment on "Basin inversion and fault reactivation in laboratory experiments". In *Journal of Structural Geology* 29 (8), pp. 1414–1416. DOI: 10.1016/j.jsg.2007.05.002.

1010   Willingshofer, E.; Neubauer, F.; Cloetingh, S. (1999): The significance of Gosau-type basins for the late cretaceous tectonic history of the Alpine-Carpathian belt. In *Physics and Chemistry of the Earth, Part A: Solid Earth and Geodesy* 24 (8), pp. 687–695. DOI: 10.1016/S1464-1895(99)00100-3.

Willingshofer, Ernst; Sokoutis, Dimitrios; Beekman, Fred; Schönebeck, Jan-Michael; Warsitzka, Michael; Rosenau, Matthias (2018): Ring shear test data of feldspar sand and quartz sand used in the Tectonic Laboratory (TecLab) at Utrecht
1015   University for experimental Earth Science applications. With assistance of Ernst Willingshofer, Dimitrios Sokoutis, Fred Beekman, Jan-Michael Schönebeck, Michael Warsitzka, Matthias Rosenau et al.

Willingshofer, Ernst; Sokoutis, Dimitrios; Burg, Jean-Pierre (2005): Lithospheric-scale analogue modelling of collision zones with a pre-existing weak zone. In *Geological Society, London, Special Publications* 243 (1), pp. 277–294. DOI: 10.1144/gsl.sp.2005.243.01.18.

1020   Yagupsky, Daniel L.; Cristallini, Ernesto O.; Fantín, Julián; Valcarce, Gonzalo Zamora; Bottesi, Germán; Varadé, Roberto (2008): Oblique half-graben inversion of the Mesozoic Neuquén Rift in the Malargüe Fold and Thrust Belt, Mendoza, Argentina: New insights from analogue models. In *Journal of Structural Geology* 30 (7), pp. 839–853. DOI: 10.1016/j.jsg.2008.03.007.

Zorlu, J. (2007): Sedimentpetrographische und geochemische Untersuchungen an unterschiedlich überprägten
1025   Triasdolomiten der Ost- und Südalpen. Doctoral thesis. Ruhr-Universität Bochum, Bochum.

Zwaan, Frank; Schreurs, Guido; Buiter, Susanne J. H.; Ferrer, Oriol; Reitano, Riccardo; Rudolf, Michael; Willingshofer, Ernst (2022): Analogue modelling of basin inversion: a review and future perspectives. In *Solid Earth* 13 (12), pp. 1859–1905. DOI: 10.5194/se-13-1859-2022.